(58)

Towards a global aerosol climatology: Preliminary trends in tropospheric aerosol amounts and corresponding impact on radiative forcing between 1950 and 1990

Ina Tegen[1]
Department of Applied Physics, Columbia University, and NASA Goddard Institute for Space Studies, New York

Dorothy Koch
Center for Climate Systems Research, Columbia University, and NASA Goddard Institute for Space Studies, New York

Andrew A. Lacis
NASA Goddard Institute for Space Studies, New York

Makiko Sato
Center for Climate Systems Research, Columbia University, and NASA Goddard Institute for Space Studies, New York

Submitted to JGR

[1]Now at Max-Planck-Institute for Biogeochemistry, Jena, Germany

Abstract

A global aerosol climatology is needed in the study of decadal temperature change due to natural and anthropogenic forcing of global climate change. A preliminary aerosol climatology has been developed from global transport models for a mixture of sulfate and carbonaceous aerosols from fossil fuel burning, including also contributions from other major aerosol types such as soil dust and sea salt. The aerosol distributions change for the period of 1950 to 1990 due to changes in emissions of SO_2 and carbon particles from fossil fuel burning. The optical thickness of fossil fuel derived aerosols increased by nearly a factor of 3 during this period, with particularly strong increase in eastern Asia over the whole time period. In countries where environmental laws came into effect since the early 1980s (e.g. US and western Europe), emissions and consequently aerosol optical thicknesses did not increase considerably after 1980, resulting in a shift in the global distribution pattern over this period. In addition to the optical thickness, aerosol single scattering albedos may have changed during this period due to different trends in absorbing black carbon and reflecting sulfate aerosols. However, due to the uncertainties in the emission trends, this change cannot be determined with any confidence. Radiative forcing of this aerosol distribution is calculated for several scenarios, resulting in a wide range of uncertainties for top-of-atmosphere (TOA) forcings. Uncertainties in the contribution of the strongly absorbing black carbon aerosol leads to a range in TOA forcings of ca. -0.5 to +0.1 Wm^{-2}, while the change in aerosol distributions between 1950 to 1990 leads to a change of -0.1 to -0.3 Wm^{-2} for fossil fuel derived aerosol with a "moderate" contribution of black carbon aerosol.

1. Introduction

Radiative forcing by tropospheric aerosols remains one of the largest uncertainties in climate variability and climate change studies [*Hansen et al.*, 1997; *Hansen et al.*, 1998]. It has been suggested that cooling caused by an increase in tropospheric aerosols

masks the effect of the increase in greenhouse gases. This masking effect could be large in industrialized regions like the eastern United States (e.g., *Karl et al.* [1995]). However, due to the lack in a well-defined global aerosol climatology, the estimates of aerosol radiative forcing are still highly uncertain. The anthropogenic aerosols that are suspected to have the largest impact on climate are sulfate (which scatters solar radiation, causing regional cooling), and black carbon aerosol (BC) which is strongly absorbing at solar wavelengths, causing atmospheric heating. The magnitude and sign of the aerosol radiative forcing depend on both aerosol optical thickness and single scattering albedo, which is determined by the distribution and chemical composition of the aerosols.

Aerosols exhibit strong geographic and seasonal variations, which produce globally uneven radiative forcing (compared to greenhouse gases). Moreover, there is a large uncertainty in aerosol radiative parameters (particularly single scattering albedo) which results in even greater uncertainty of the (direct) radiative forcing due to aerosols. Producing perhaps even more uncertainty is the indirect effect of aerosols on cloud radiative properties, a topic which is beyond the scope of this paper, but for which nevertheless a definitive aerosol climatology is a necessary precursor.

In the future, new satellite instruments like MODIS, MISR, and EOSP are expected to improve our understanding of the global aerosol distribution. However, for now the possibilities of deriving an aerosol climatology from satellite observations are limited. So far, estimates of tropospheric aerosol forcing and climate effects rely on aerosol distributions derived from transport models (e.g., *Tegen et al.* [1996] for soil dust). Most estimates of this kind exist for sulfate aerosols [e.g., *Charlson et al.*, 1991; *Kiehl and Briegleb*, 1993; *Kiehl and Rodhe*, 1995; *Roeckner et al.*, 1995]. Recently, several studies investigated the radiative forcing for a mixture of sulfate and black carbon aerosols [*Haywood et al.*, 1997; *Haywood and Ramaswamy*, 1998; *Schulz et al.*, 1998; *Penner et al.*, 1998; *Mhyre et al.*, 1999]. The tropospheric aerosol top-of-atmosphere (TOA)

forcings found in these studies ranged from -0.4 to +0.1 Wm^{-2}. In the study of *Penner et al.* [1998], the authors estimated the radiative forcing of a mixture of sulfate, black carbon and organic carbon aerosols from fossil fuel and biomass burning, they estimated forcings ranging from -0.30 to -0.88 Wm^{-2}. Those ranges in TOA forcings reflect some of the uncertainties in such estimates.

Those estimates result from taking the difference between radiative fluxes obtained with an aerosol distribution from a reference year and the "preindustrial" case with no anthropogenic aerosols present. However, considerable changes in aerosol distributions may have taken place during the last decade. Since the 1950s, global SO_2 emissions (SO_2 is a precursor of sulfate aerosol) increased considerably with different rates for different countries [*Lefohn et al.*, 1999]. Not only changes in total aerosol optical thickness, but also changes in aerosol composition may have occurred, since SO_2 emissions were considerably curbed in USA and western Europe since the early 1980s due to environmental regulations like the "Clean Air Act". The emissions of black carbon particles may not have been reduced as effectively in those regions, although they may have been reduced by changes in the fossil fuel burning technology. In other parts of the world, like China, SO_2 emissions and therefore presumably sulfate aerosol concentrations, increased strongly during the whole period since 1950.

Here we present an estimate of changes in sulfate, BC and organic aerosols from fossil fuel burning from 1950 to 1990, together with an estimate of how these changes affect the tropospheric aerosol properties and direct radiative forcing. The resulting distributions of tropospheric aerosols are designed for use in climate change studies.

2. Aerosol Distributions

2.1. Aerosol Emissions from Fossil Fuel Burning

2.1.1. Sulfate

Several estimates of global emissions of sulfur dioxide, the precursor for sulfate aerosol, are available. A detailed emission scenario for the year 1985 has been developed by *Benkovitz et al.* [1996]. *Dignon and Hameed* [1989] estimated global sulfur emission trends from 1860 to 1980 by correlating sulfur emission data with liquid and solid fossil fuel use data for OECD and non-OECD countries. A different database of global sulfur emissions, which is used in this investigation, has been developed by *Lefohn et al.* [1999], who estimated historical global sulfur emission for the years 1850 to 1990 by using statistical data on fossil fuel use (equaling production plus import minus export with fuel consumption). They computed sulfur emissions for each country by multiplying the net fuel use with the sulfur content of the fuel and by a factor incorporating sulfur retention, thus obtaining sulfur emissions per year and country. Additionally, SO_2 emissions from metal production were taken into account. Specifically, they considered flue gas desulfurization controls in coal burning facilities, as well as low-sulfur coal switching strategies, which were implemented in 1973 in the United States. To obtain higher resolved geographical distributions, we weighted the emission data, which are given by country, with the population density for each country on a 1° by 1° grid. Figure 1a shows the sulfur emissions from *Lefohn et al.* [1999] for the global average and for the examples of the countries USA and China for the years 1950 to 1990. While during that period the global increase in sulfur emissions was almost linear, with a drop between 1980 and 1985, the sulfur emissions in China increased more strongly. In the United States, on the other hand, sulfur emissions have slightly decreased since the late 1970s. The sulfur emission trend for countries in western Europe, another major source region, is similar as the trend for the USA. One of the largest uncertainties in

this emission database is the actual sulfur content of the fossil fuels. Based on the data given in *Lefohn et al.* [1999], the uncertainty in sulfur emissions is estimated to be 25% in the global mean (see Figure 1a), with a range of 5% to 80% for individual countries. Globally, the sulfur emission values for the reference year 1985 from this work agree very well with the widely used sulfur emission dataset from *Benkovitz et al.* [1996] (S emissions in 1985 are ca. 65 Mt/yr in both studies [*Lefohn et al.*, 1999]), although there are some regional differences.

2.1.2. Black carbon

We used the method described by *Cooke and Wilson* [1996] (CW96) to derive global black carbon (BC) emissions from fossil fuel burning from the UN energy statistics database [*United Nations*, 1996]. While the authors extracted global black carbon emissions specifically for the year 1984, we applied a simplified version of their method for the period 1950 to 1994, which is the full period for which data from the UN statistics database are available. CW96 calculated fuel use as the difference of the sum of fuel production and imports and the sum of exports and stock changes for each country. BC emissions were calculated by multiplying the amount of fuel use with emission factors from the literature for domestic and industrial burning for 126 fuel types. In a more recent detailed study of global BC emissions, *Cooke et al.* [1999] took into account the level of development for calculating emissions from a country, thus updating the CW96 BC emissions database. However, considering the large uncertainties in BC emissions, we used the simpler CW96 method. The results from applying this method can be regarded as an upper limit for global BC emissions, since the emission factors used in the more recent study are lower. Also, *Bond et al.* [1998] found emission factors of light-absorbing particles from a lignite power plant that were lower by a factor of 6.5 than the factor used in the *Cooke et al.* [1999] study, which would further decrease BC emissions by ca. 50% if applied globally.

In the simplified version, we considered only the consumption of hard coal, brown coal and diesel, since the burning of these fuels are the main sources for BC aerosol. Following CW96, we assumed emission factors of 10 g BC/kg fuel for domestic burning of hard coal and brown coal, 1 g BC/kg fuel for industrial coal burning, 2 g BC/kg for domestic and 0.7 g BC/kg for industrial diesel fuel burning. Information about the percentage of domestic vs. industrial fuel use were missing for several countries in the UN energy statistics. Therefore, all countries were grouped into 9 regions with similar geographic location and political/economical systems. Those were Africa, Centrally Planned Asia, Centrally Planned Europe, Developing America, Far East, Middle East, North America, Oceania, and Western Europe, as defined by *Boden et al.* [1996]. Average emission factors were calculated for the countries in each region and the years for which the information on relative contribution of domestic and industrial burning to the use of the individual fuel types was available. Those were then applied for those countries and years where only information about total fuel use was available. These emission factors in effect replace the 'combined' emission for industrial and domestic fuel burning used by CW96. This simplification of the method of CW96 results in global BC emissions of 8.3 Mt/yr for the year 1984, which agrees very well with the emission of 8.0 Mt/yr calculated by CW96. The newer estimate by *Cooke et al.* [1999] results in a lower global annual emission of BC aerosol of 6.4 Mt/yr.

The resulting trend in BC emissions reflects the trend in the total fossil fuel use, and the shifts between the use of coal and diesel fuel. Since the percentage of fuel use in domestic vs. industrial sectors was not reported for years before 1970, we assumed the same relation between domestic and industrial fuel burning as for the average of the years 1970 to 1994. An additional decrease in BC emissions may have occurred due to shifts from domestic to industrial use of the individual fuel types ('trend' case). For most regions we could estimate this trend by extrapolating the percent burning in the industrial sector back that was found in the period 1970 to 1990 back to the year 1950.

For those regions - specifically Western Europe, which experienced a shift from domestic to industrial burning - this results in a different BC emission trend.

In Figures 1b and 1c annual BC emissions are compared for the cases that include the shift in relative contribution of domestic vs. industrial burning, and the case of BC emissions resulting from an average value for this percentage. These emissions are shown for the global average and for the example of Germany, where the difference due to this shift is high. The additional uncertainties in BC emissions from this shift between domestic and industrial fuel use are small compared to the uncertainties resulting from uncertainties in the emission factors.

Figure 1b shows the resulting trend and uncertainty range for BC emissions for the globe. The uncertainty range has been estimated from the standard deviation for the distribution of domestic and industrial fuel use in the individual regions, and a rather arbitrary uncertainty of 50% for the emission factors. As mentioned before, this may give a too small uncertainty range (at the lower end), since there is additional uncertainty in these numbers from the fact that we did not include an estimate of the changes in BC emissions due to changes in fossil fuel burning technology. Figure 1c shows the examples of BC emissions for the countries USA, China, and Germany. From these calculations the resulting trend in global BC emission is steeper than linear for the 'no-trend' case (which is also the case for for S emissions). In both USA and China, BC emissions increased over the whole period 1950 to 1990. For the 'trend' case, the global BC emissions increase almost linearly during this period. This is due to the shift from domestic to industrial burning in those regions that have high emissions (North America, Europe), with the resulting decrease in BC emission factors counteracting the effect of increasing fossil fuel burning on BC emissions.

Figure 2 shows the ratio of S and BC emissions for the global average, together with the ratios for China and USA. For the global mean, the trend of this ratio during the years 1950-1990 depends on whether the shift from domestic to industrial burning

in taken into consideration (for that case, this ratio slightly increased in the global mean) or not (in which case the ratio decreased in the global mean). For countries with limitations on sulfur emissions this ratio clearly decreased; for the example of the USA it decreased by ca. 30% from 1950 to 1990. This trend may affect the aerosol optical properties. On the other hand, in countries with no such regulations on SO_2 emissions the ratio stays approximately at the same level, as in the example of China.

Emission factors from the CW96 study were high compared to the revised study by *Cooke et al.* [1999]. Also, the use of the upper limit of the BC emission uncertainty range shown in Figure 1b would lead to unrealistically high BC concentrations. Therefore, we regarded the results for global BC emission obtained by this method as an upper limit. Like for the case of SO_2 emissions, the distribution of BC emissions on a 1° by 1° map was obtained by weighting the emissions that are calculated for each country with the population density distribution.

2.1.3. Organic aerosol

Organic carbonaceous aerosol (OC) is the less absorbing, chemically reactive part of the carbon containing aerosol. Organic aerosol can be emitted from fossil fuel burning, from biomass burning, or as natural emissions from plants (e.g. terpenes). For the purpose of estimating an aerosol trend from 1950 to 1990, here we are mainly interested in the trend in organic aerosol emissions from fossil fuel burning. Very little information is available on these emissions, although the recent TARFOX experiment showed a strong contribution of organic aerosols to the total aerosol scattering off the coast of the Eastern US [*Hegg et al.*, 1997]. Since even less information on OC emissions and concentrations is available compared to BC aerosol, we obtained OC emissions by multiplying BC emissions by a factor of 4 (as done by e.g. *Liousse et al.* [1996] and *Penner et al.* [1998]). Using this factor, the resulting organic aerosol mass load (derived with a transport model, see below) in the TARFOX area is of the same magnitude as

the sulfate content at that location (using the sulfate distribution calculated by *Koch et al.* [1999]). As for the BC emissions, this method results probably an upper limit for global OC emissions, since it is based on the upper limit estimate for BC emissions. Also, some of the organic aerosol detected during the TARFOX campaign may have originated from plant emissions instead of fossil fuel burning. To estimate a lower limit for the organic aerosol emissions from fossil fuel burning is difficult without more constraints. To make an estimate of the full range of uncertainties for OC emissions, we assume the lower limit for OC emissions from fossil fuel burning to be zero.

2.2. Aerosol Distribution and Optical Thickness

2.2.1. Sulfate

From the global emission fields, aerosol distributions are calculated using previously described aerosol transport/chemistry models. The global annual SO_2 emissions were averaged over 10 year periods and resulting aerosol distributions were calculated for the years 1950, 1960, 1970, 1980 and 1990. The sulfate aerosol distributions for individual years were obtained by interpolating the average decadal distribution to obtain the regional distribution. For each year the concentrations were then scaled with the global emissions of SO_2 for that particular year.

Sulfate distributions were obtained with the model of *Koch et al.* [1999], who calculated sulfate chemistry and transport on-line in the GISS GCM. The chemistry model includes prognostic H_2O_2 as in-cloud oxidant, together with OH, DMS, MSA, SO_2 and sulfate. Unlike the sulfate precursor SO_2, the oxidants are kept constant over the years in these calculations. The anthropogenic increase in SO_2 emission translates directly into an increase in sulfate aerosol loads. The GCM was integrated for 6 model years, and the resulting SO_4 concentrations from the last 5 years were averaged. The *Koch et al.* [1999] sulfate model, using SO_2 emissions of *Benkovitz et al.* [1996], has been validated by extensive comparisons with observations of surface concentrations of SO_4

and SO_2, as well as sulfur deposition.

Validating the long-term trend in sulfate concentrations is problematic, since it requires comparison with measurements taken over a multi-year period, ideally more than 10 years. An increasing trend in sulfate concentrations since 1950 can be found in Greenland ice cores [*Mosher et al.*, 1993; *Mayewski et al.*, 1990]. From measurements of sulfate concentration at a Greenland ice core near Dye 3, *Mayewski et al.* [1990] find that the increase in sulfate at this location is most similar to the trend in SO_2 emission increase in the USA (concluding that this is the primary source for sulfate in south Greenland). However, it is difficult to interpret such data from the remote site at Greenland, since those data do not represent hemispherical values. Due to the short lifetime of aerosols, changes in transport and local effects can influence the signal in the ice cores.

The decrease in sulfate deposition in the United States is reflected in the observations from the National Acid Deposition Program/National Trends Network (NADP/NTS) assessment for the years 1979 to present [*NADP*, 1999]. Figure 3 shows a comparison of model results with the sulfur deposition fluxes, averaged for the continental US. The network measurements started in 1979 with 24 stations, the number increased to 181 stations in the year 1996. The modeled sulfur deposition lies below the observations until the mid-1980s, but there is agreement in the trend in sulfur depositions for model and observations. A strong decrease in sulfur deposition exists in the beginning of the 1980s, leveling off in the late 1980s.

In western Europe, long-term sulfate measurements exist from the network of the Cooperative Program for Monitoring and Evaluation of the Long Range Transmission of Air Pollution in Europe (EMEP) [e.g., *Schaug et al.*, 1987] since the late 1970s for 32 EMEP sites. Figure 4a shows a comparison of sulfate concentration measurements with the model results for 32 EMEP stations, which are subdivided for 17 "central" European stations (south of 55°N) (Figure 4b) and 15 "northern" (north of 55°N)

stations (Figure 4c). As for the comparison with the NADP measurements, the trend of sulfate concentrations is reproduced over the years, with a decrease between 1980 and 1990. The decreasing trend is stronger for the "central" European stations, where the model overestimates total sulfate concentrations. On the other hand, the agreement of the model with the observations is very good for the "northern" European stations. The decreasing trend in sulfate concentrations between 1980 and 1990 is not as strong at those stations, compared to the European average.

The modeled sulfate aerosol mass loads were converted into aerosol optical thicknesses τ by taking into account the hygroscopic growth of the sulfate particles, using the formulation of *Charlson et al.* [1984] $\tau = mB(\mathrm{RH})$. (m is the sulfate mass load in g/m^2, B(RH)= 5m^2/g $\times$ f(RH), where f(RH)accounts for the effect of relative humidity on the optical thickness.) B(RH) is capped at 2.5 for RH$>$ 85%.

2.2.2. Black and organic carbon aerosols

Black carbon and organic aerosol distributions were calculated using the GISS tracer transport model. For present day conditions, the results were described by *Hollrigl* [1997]. The model is based on the GISS aerosol model described in *Tegen and Fung* [1994] for soil dust aerosol. In order to estimate the maximum contribution of carbonaceous aerosol to the tropospheric aerosol load, we assumed BC and OC particles to be insoluble, not being able to form cloud condensation nuclei and be removed by in-cloud scavenging. Since OC may be partly soluble and BC may become coated by sulfate aerosol, and consequently become increasingly soluble during transport, this means that wet deposition probably underestimated by this method.

Carbonaceous aerosol concentrations from this model using the high emission and low deposition estimates can be regarded as an upper limit. For this case, the atmospheric lifetime for BC is ca. 15 days, and the resulting BC mass load for this case is 0.7 mg/m^2. This is approximately 5 times higher than the estimates from

Liousse et al. [1996] and *Cooke et al.* [1999]. In the latter study it was assumed that carbonaceous particles are partly emitted as hydrophilic aerosol, and hydrophobic particles change into hydrophilic with a lifetime of ca. 1 day. Since little information exists about such conversion rates, which would depend on the presence of hydrophilic substances like sulfuric acid, we decreased the BC load obtained by our model by a factor of 2 ("moderate BC" case) and 5 ("low BC" case) for sensitivity studies which would approximately cover the range of uncertainties in the atmospheric BC load. For these cases, the OC load was lowered by these factors as well.

Figures 5a and 5b shows the comparison of BC concentrations for the "moderate BC" case with measurements from various authors, summarized by *Liousse et al.* [1996], and the comparison of BC and OC aerosol concentrations with stations from the IMPROVE network in the United States [*Malm et al.*, 1994], respectively. For Figure 5a, only northern hemisphere data were compared to the model results since we were evaluating the BC distribution from fossil fuel emissions, and assume biomass burning contribution to be small in these locations. Figure 5a shows reasonable agreement between model results at remote stations. For ocean stations some scattering exists, while for this "moderate BC" case the model generally underestimates the BC concentrations at rural stations - at those locations the "maximum BC" case gives good agreement. Similarly, for the U.S. stations (which are also "rural" stations) (Figure 5b) the model underestimates BC and OC concentrations for the "moderate" case; the "maximum" BC case would give better agreement.

While for sulfate aerosol some long term observations exist (which were supported in response to concerns about "acid rain") we are not aware of any long-term measurements of carbonaceous aerosols. The trend for this aerosol type remains therefore highly uncertain.

BC and OC aerosol were converted into optical thicknesses using $\tau = mB$ by using specific extinction cross sections B of 9 m^2/g and 8 m^2/g (see *Liousse et al.* [1996]),

respectively. Possible changes in optical thickness due to a change in hygroscopic growth of carbonaceous particles were not taken into account.

2.3. Other Aerosol Types

Above we described the estimated trend in emissions of aerosols from fossil fuel burning. Additional aerosol types are important for the consideration of the impact of tropospheric aerosol on the radiation balance. The main aerosol types additional to those described above that were included as part of the global aerosol climatology are soil dust, sea salt, natural sulfate, natural organics, and biomass burning aerosol.

Soil dust aerosol is partly a natural aerosol, but part of the dust load in the atmosphere may be originating from anthropogenically disturbed soils; this part may contribute up to 50% to the atmospheric dust load [*Tegen and Fung*, 1995; *Tegen et al.*, 1996]. Dust has a strong interannual variability. Changes in dust sources can be caused by changes in meteorological parameters like surface wind speed and precipitation, as well as in surface conditions like a change in the vegetation cover which protects the soil surface from wind erosion. It has been speculated that interannual variability in dust loads in specific regions may be correlated with climate modes like ENSO [*Prospero and Nees*, 1986] or NAO [*Moulin et al.*, 1997], but such relationships have not yet been firmly established. Also, the contribution of disturbed sources to the total dust load is uncertain, and the change in this contribution is undefined. Therefore, dust was assumed to be constant during 1950-1990. We used the model derived distribution from *Tegen and Fung* [1995] to describe the monthly dust distribution for 8 different particle size classes between 0.1 and 10 μm and dust optical thickness derived from the concentration and size distribution of the dust, as described by *Tegen and Lacis* [1996].

Sea salt is a natural background aerosol without anthropogenic component, and its mass load is not expected to vary considerably form year to year. Although the concentrations may change regionally with changing wind speeds and precipitation, the

source area remains virtually unchanged. To describe the background distribution, the global monthly distribution from *Tegen et al.* [1997] is used, with assuming a higher specific scattering cross section B of 2.5 m^2/g following the suggestions by *Quinn and Coffman* [1999] and *Haywood et al.* [1999] for the calculation of sea salt optical thickness.

Natural sulfate aerosol distribution and optical thickness from DMS emissions has been calculated by *Koch et al.* [1999]. The optical thickness calculation takes into account the particle growth by specific humidity as for the case of anthropogenic sulfate.

Biomass burning aerosol is assumed to be of mainly anthropogenic origin. It also has a strong interannual variability with higher burning during dry years (i.e. Indonesian forest fires during El Nino years), and changes in burning rates. However, due to missing information on these changes we assume this contribution to be constant over the years. We used the monthly biomass burning distribution, as well as the distribution of natural organics from *Liousse et al.* [1996]. Optical thickness was calculated as for the BC and OC aerosols from fossil fuel burning, using specific extinction cross sections B of 9 m^2/g and 8 m^2/g, for BC and OC, respectively.

Thus, monthly sea salt, soil dust, natural sulfate, natural organics, and biomass burning aerosol distributions are kept constant over the years 1950 to 1990, but are included in the calculation of global aerosol optical thickness and single scattering albedo. Plate 1 shows global distributions of the annually averaged optical thicknesses of the individual aerosol types for the year 1990. The differences in the regional distributions indicate that the optical properties of the aerosol mix may vary widely for different regions.

Plate 2 shows the global averaged seasonal aerosol optical thickness variations for soil dust and non-dust tropospheric aerosols. For all aerosol types there is a pronounced summer maximum in optical thickness. Included for comparison is the stratospheric volcanic aerosol [*Sato et al.*, 1993] which must also be included for completeness in defining the radiative forcing over past decades [*Hansen et al.*, 1997; *Hansen et al.*,

1998].

3. Total Tropospheric Aerosol Optical Thickness

From the aerosol distributions described above, the total tropospheric aerosol optical thickness τ was calculated at 0.55 μm wavelength for an external mixture of the tropospheric aerosols. Tropospheric aerosol optical thickness is the sum of the optical thicknesses τ_i of the individual aerosol types, which are summarized for the global annual mean in Table 1. Figure 6 shows the resulting distribution of tropospheric aerosol optical thickness for the years 1950, 1970, and 1990 for the major aerosol types described above, which include natural and anthropogenic sulfate, BC and OC from fossil fuel burning, biomass burning aerosols, natural organics, soil dust and sea salt. Changes in the aerosol optical thickness are caused by changes in fossil fuel emissions. As expected from the emission trend, the optical thickness increased strongly in Asia for this time period. In western Europe, optical thickness increased between 1950 and 1970 and slightly decreased between 1970 and 1990, while in the US a slight increase is found between 1970 and 1990. For the examples of China and US this trend is also shown together with the global trend in Figure 7. There, the modeled annual optical thicknesses trends are shown for the whole period 1950 to 1990. According to this estimate, the globally averaged optical thickness increased by 0.025 during this period, while in China, the optical thickness nearly doubled. This shift in the global tropospheric aerosol distribution pattern may possibly be causing changes in climate response to the aerosol forcing.

4. Single Scattering Albedo

The tropospheric aerosol single scattering albedo ω_0 at 0.55 μm wavelength was calculated as

$$\omega_0 = \frac{\sum_{i=1}^{n} \tau_i \omega_{0i}}{\sum_{i=1}^{n} \tau_i}$$

where τ_i and ω_{0i} are the extinction optical thickness and single scattering albedo of the individual aerosol types, respectively. This calculation included all aerosol types described above, and was based on the monthly mean optical thicknesses. The single scattering albedos for the individual aerosol types that were used for this calculation are summarized in Table 1, together with the global annual average optical thicknesses.

In Figure 8, single scattering albedos that result from the model are compared to measurements at various locations by different authors as summarized by *Heintzenberg et al.* [1997]. Additionally shown are values for the recent TARFOX field study off the coast of the northeastern US [*Hegg et al.*, 1997] and for the SCAR-B [*Hobbs et al.*, 1997] field experiment during burning season in the Brazilian Amazon. Instead of the aerosol single scattering albedo of the total atmospheric column we compared with model results from the first atmospheric layer. The symbols represent model results for the "moderate" carbonaceous aerosol case (BC and OC aerosol both 0.5 times the maximum), the error bars indicate the results obtained for "maximum BC" (lower limit of the modeled single scattering albedo) and the "low BC" case (upper limit). The results show some spread as can be expected for such a comparison; for most cases the "moderate" or the "maximum" agree better with the observations than the "low BC" case. The model still considerably overestimates the single scattering albedo in the Brazilian Amazon during burning season, while the "maximum BC" case agrees well with the aerosol single scattering albedo observed during TARFOX.

Heintzenberg et al. [1997] also shows results for the latitudinal change in single scattering albedo during the RITS88 cruise in March 88 in the central Pacific from

Dutch Harbor, Alaska, to Samoa. They observed minimum single scattering albedo of ca. 0.92 at ca. 45°N, which increases to values of ca. 1.0 around 5°N to 10°S. In the model, the minimum single scattering albedo of 0.93 occurs around 25°N, the values increase to 0.99 at the Equator. While the modeled minimum and maximum single scattering albedo in this part of the Globe agrees quite well with the observations, the location of the minimum is located further south than in the real world, reflecting some differences in the atmospheric transport.

Figure 9a-c shows the global distribution of single scattering albedo of all tropospheric aerosols for the year 1990, for the cases of maximum, moderate, and low carbonaceous aerosol contribution. The global and annual averaged single scattering albedo for these cases is 0.934, 0.945, and 0.954, respectively. Regions of low single scattering albedo (as low as 0.89 in some locations in the annual mean) are determined mainly by the BC and soil dust aerosol distributions. In the case of soil dust, the single scattering albedo of average 0.89 is uncertain and may actually be underestimated in several locations. In these calculations refractive indices for far-traveled Saharan dust measured by *Patterson et al.* [1977] were used to obtain dust optical properties, this may introduce considerable errors if applied to dust from other locations, like Asia or Australia. Over the southern oceans the single scattering albedo is as high as 0.99 since major sources of absorbing aerosols are absent. At high latitude regions near the North- and South pole the single scattering albedo decreases, since the more reflecting sulfate aerosols are more efficiently removed during transport than the more absorbing carbonaceous aerosols.

Figure 10 shows the trend in the annual average tropospheric aerosol single scattering albedo for the years 1950 to 1990 for the "moderate" BC case, again for the global mean and for the examples of USA and China. These calculations result in a slight decrease in global average and USA average single scattering albedos, while a slight increase is obtained for single scattering albedos in China. However, since

the contribution and change in absorbing aerosol is very uncertain, this change is not significant.

5. Aerosol Radiative Forcing

The radiative effect of the tropospheric aerosol distributions described above was calculated by using the radiation model that is embedded in the GISS GCM [*Hansen and Travis*, 1974; *Hansen et al.*, 1983; *Lacis and Mishchenko*, 1995]. Radiative properties (extinction efficiency and asymmetry parameter, in addition to single scattering albedo) are wavelength dependent, and depend on effective particle size and the wavelength dependent complex refractive indices. They were calculated using Mie scattering for the standard Γ size distribution with the effective variance 0.2 for each particle type. Refractive indices used here were from measurements of ammonium sulfate by *Toon and Khare* [1976] for sulfate aerosol, measurements of soot aerosol and sea salt [*Nilsson*, 1979] for BC and sea salt aerosol, respectively, and soil dust measurements by *Patterson et al.* [1977] and *Volz* [1973]. For organic aerosol, the wavelength dependent refractive indices of ammonium sulfate by *Toon and Khare* [1976] was used, with the single scattering albedo limited to 0.96 for fossil fuel derived organic aerosols, 0.98 for natural organics and 0.93 for organic aerosols from biomass burning. Reflection, absorption and transmission of the different aerosol types are calculated using the single gauss point doubling/adding radiative transfer model in the GISS GCM, with using the correlated k-distribution method to compute absorption by gases and particles for 6 solar and 25 thermal intervals. Instantaneous radiative forcing and changes in atmospheric heating due to tropospheric aerosols were calculated for the following cases:

FF 90: Fossil fuel aerosols only, moderate carbonaceous aerosol (BC and OC half of the maximum optical thickness), year 1990

FF 80: As above, year 1980

FF 70: As above, year 1970

FF 50: As above, year 1950

Max C: Fossil fuel aerosols only, maximum BC and OC optical thicknesses (1990)

Min C: Fossil fuel aerosols only, BC and OC optical thicknesses one-fifth of maximum (1990)

Max τ: Fossil fuel aerosols only, maximum sulfate, maximum OC, BC 0.72 times maximum (1990) (see below)

Min τ: Fossil fuel aerosols only, minimum sulfate, no OC, BC 0.42 times maximum (1990) (see below)

All A: Case FF 90 plus biomass burning aerosols plus anthropogenic dust

All T: All tropospheric aerosols (fossil fuel: case FF 90)

Radiative forcing was calculated for the years 1950 to 1990 for the case of "moderate" carbonaceous aerosol contribution (cases FF 90 - FF 50), together with test cases where the contribution of carbonaceous aerosol was maximum (Max C), and the case of "low" carbonaceous aerosol (Min C), as well as for the case of maximum and minimum aerosol optical thickness (Max τ and Min τ). Those latter cases were constructed by choosing the maximum and minimum sulfate aerosol optical thicknesses that are resulting from maximum and minimum SO_2 emissions, together with maximum and minimum contributions of organic aerosols. The minimum contribution of fossil fuel derived organic aerosols was assumed to be zero, since the uncertainties in the loads of this aerosol type are very high. For these maximum and minimum optical thickness cases, the fossil fuel black carbon contribution chosen to have a value which resulted in a global annual average single scattering albedo for all tropospheric aerosols of 0.945, which is the same value as the case of "moderate" black carbon contribution. This

condition requires 0.72 and 0.42 times the "maximum" BC optical thickness for the maximum and minimum optical thickness case, respectively. In addition to the average forcings for the fossil fuel aerosol scenarios, we also calculated the TOA forcing and atmospheric heating caused by all anthropogenic aerosols (including biomass burning and anthropogenic dust, case "all A"); as well as the change in TOA radiative flux caused by all tropospheric aerosols (i.e. including sea salt, natural dust, natural sulfate and natural organics, case "all T"). Those calculations were carried out for the "moderate" case for the year 1990. The radiative forcing was calculated by running the GISS GCM for one model year without the specified aerosol distribution. It was then re-run for the model year with the different aerosol scenarios, with the atmospheric circulation and cloud optical properties and water vapor prescribed by the no-aerosol experiment. The instantaneous forcing was calculated as the difference between the modeled radiative fluxes with the different aerosol scenarios and the no-aerosol experiment.

6. Results

The resulting global average values for TOA radiative forcing and changes in radiative heating due to fossil fuel aerosols for the different scenarios are summarized in Table 2, together with annual average values for optical thickness and the single scattering albedo. The latter is an average for all tropospheric aerosols in each case, not only the fossil fuel derived aerosols. For the case of a "moderate" contribution of carbonaceous aerosol (OC and BC 0.5 times the maximum case, FF 50 - FF 90), the fossil fuel aerosol optical thickness increased substantially from 0.014 to 0.039 from the years 1950 to 1990. For the sum of all tropospheric aerosols, the optical thickness increased from 0.097 to 0.122 over this period. The globally averaged single scattering albedo for tropospheric aerosols decreases only slightly by 0.004 for this period. For the case of maximum carbonaceous aerosol contribution, the change in globally averaged single scattering albedo is more substantial. In that case, the global averaged single

scattering albedo decreases by 0.01 from 0.944 in 1950 to 0.934 in 1990. The change in the global averaged optical thickness for the moderate case (an increase of 0.025 from 1950 to 1990) is of the same order of magnitude as the difference in optical thickness for the maximum and minimum BC scenarios, and smaller than the difference for the maximum and minimum optical thickness scenarios. However, the global average numbers do not take into account that the regional distribution of the fossil fuels derived aerosols shifted considerably over this time period.

Changes in fossil fuel aerosol from 1950 to 1990 causes a decrease by ca. 0.2 Wm^{-2} in TOA radiative forcing and an increase in atmospheric heating by ca. 1 Wm^{-2} (cases FF 50 to FF 90). For these cases, the TOA forcings are negative. The relatively small numbers are caused by cancellation of positive and negative solar forcing values over bright and dark surfaces in the global average. The atmospheric heating (calculated as the difference between TOA and surface forcing) shows the amount of energy absorbed in the atmospheric column due to the instantaneous forcing. The large values indicate the important role of absorbing (black carbon) aerosols.

The differences between the maximum and minimum BC cases are ca. 0.6 Wm^{-2} for TOA forcings and 1.5 Wm^{-2} in atmospheric heating. The maximum BC case is the only scenario where the TOA forcing of fossil fuel aerosols results in a positive global average value. The large uncertainty in aerosol single scattering albedo leads to the high uncertainty in the forcing estimates. The differences between the maximum and minimum optical thickness cases is ca 0.2 Wm^{-2} for TOA forcings and 1 Wm^{-2} for the atmospheric heating. These values are similar to the differences obtained for the "moderate" scenario for the time period 1950 to 1990, although the difference for the maximum and minimum optical thickness cases is 0.040, which is almost twice the difference between the 1950 and 1990 case, which is 0.025. This difference can be explained by the additional slight change in single scattering albedos and the shift in the aerosol distribution pattern over the years 1950 to 1990. If we compare the

case of industrial aerosol forcing for 1990 for the moderate case (FF 90) with forcing due to all anthropogenic aerosols (including biomass burning and anthropogenic dust) (case "All A"), TOA forcing changes to a positive value, and the atmospheric heating increases by 1 Wm^{-2}. The positive forcing in this case is due to the contribution of absorbing biomass burning and dust aerosol over bright desert surface, together with the contribution of thermal forcing from the large dust aerosols. Additional large uncertainties are connected with the estimates of those additional anthropogenic aerosol types. All aerosols (anthropogenic plus natural, case "all T") cause a negative TOA forcing of -0.85 Wm^{-2} for the 1990 "moderate" aerosol case, since the natural aerosols (sea salt, natural sulfates, natural organics) are mainly non-absorbing.

The aerosol radiative forcing was calculated by treating the aerosols as an external mixture, according to *Haywood and Shine* [1995] the absorption due to aerosols increases for an internal mixture of black carbon and sulfate, which could cause a 20-60% decrease in TOA forcing.

The resulting range in TOA forcings considering the uncertainties in the aerosol distribution and optical properties agrees with the range of TOA forcings of other recent investigations of mixtures of sulfate and carbonaceous aerosols. Several studies found global average TOA forcing values for mixtures of BC and sulfate aerosols that lie within a close range: *Schult et al.* [1997] find TOA forcing of -0.2 Wm^{-2} for an external mixture of fossil fuel BC and sulfate; while *Haywood et al.* [1997] found a TOA forcing of -0.18 Wm^{-2} for externally and 0.02 Wm^{-2} for internally mixed fossil fuel derived black carbon and sulfate aerosol. For those same cases *Mhyre et al.* [1999] found forcings of -0.16 Wm^{-2} and -0.10 Wm^{-2}, respectively. The close agreement between the latter two studies may not be that surprising, since both made the simplified assumption of a fixed ratio of 0.075 between BC and sulfate aerosols. *Penner et al.* [1998] found a range of TOA forcings of -0.35 to -0.65 Wm^{-2} for externally mixed fossil fuel aerosols (including OC) and a range of -0.49 - -0.88 Wm^{-2} if also including biomass burning

aerosols. Those results show a stronger negative forcing than for our reference case FF 90 with "moderate" carbonaceous aerosols. *Penner et al.* [1998] also show changes in atmospheric heating due to fossil fuel BC and OC; their resulting value of 0.92 Wm^{-2} agrees quite well with the value of 0.91 Wm^{-2} we obtain for the "moderate BC" fossil fuel aerosol distribution for the year 1980 (FF 80).

Differences in the global average values for TOA forcings do not necessarily reflect differences in the regional forcings, since regional changes in positive and negative forcings may cancel if averaged over the globe. Plate 3a shows the regional distribution of the TOA net forcing due to industrial aerosols for the year 1980, which shows that in this case the forcing is mostly negative. Plates 3b and 3c show the changes in forcing between the years 1970 and 1990 for the cases of maximum and minimum contribution of carbonaceous aerosols. These changes can result in either increase or decrease of the average forcing. While the change in global mean forcing during this period is small for TOA forcing (-0.2 to +0.1 W m^{-2}), the regional increase in forcing can be up to 4.2 W m^{-2} for the maximum BC and -2.1 W m^{-2} for the minimum BC case. The change in global mean atmospheric heating for these cases can also vary substantially between -0.4 and 1.2 W m^{-2} for the period 1970 to 1990 for the extreme cases of BC contribution.

7. Conclusions

There is little doubt that the presence of strongly absorbing (black carbon) aerosol decreases the negative TOA aerosol direct radiative forcing compared to the forcing by sulfate aerosol alone. However, there is considerable uncertainty in those estimates due to uncertainties in the aerosol distribution, size distribution, and chemical composition of the aerosol mixture. In addition to the uncertainties in optical thickness and optical properties of tropospheric aerosols, the decadal change in their distribution should be taken into account for climate change studies. For the period 1950 to 1990, the global optical thickness of aerosols from fossil fuel burning increased by nearly a factor of 3

according to estimates of the increase in emissions of SO_2 and carbonaceous aerosols from fossil fuel burning. Due to this increase, the total tropospheric aerosol optical thickness (including natural aerosols) increased by about 25% over this period. The rate of increase in the aerosol optical thickness is different for different parts of the globe. In China, the aerosol optical thickness increase was especially strong due to the increase in fossil fuel emissions, while in the USA and western Europe SO_2 emissions leveled since the early 1980s due to emission controls. For emissions of black carbon aerosol, similar changes are assumed as for SO_2 emissions. However, for this aerosol type changes are more difficult to estimate. In addition to changes in coal and diesel use (the main sources of black carbon particles from fossil fuel burning), advances in filter technology would lead to a decrease of particle emissions, which has not been considered in these estimates. Different rates of emission trends for sulfate and BC aerosol would lead to changes in optical properties, which are regionally different. However, since the information for such trends is scare for BC aerosols (while reasonably well known for sulfate), we cannot be certain about direction of the relative contribution of BC and sulfate to the total aerosol load. Although we can estimate the regional trends in fossil fuel derived aerosol optical thickness with some confidence, the change in single scattering albedo (which determines the change in TOA radiative forcing and the sign of this forcing) is unclear. Nevertheless, it is important to consider the changes in tropospheric aerosol distributions for long-term climate change experiments. Changes in TOA optical thickness magnitudes and distribution patterns result in changes in TOA forcing and atmospheric heating, which are of the same magnitude as the uncertainties in forcing due to uncertainties in total optical thickness and single scattering albedos (especially considering the use of quite extreme assumptions to asses these uncertainties). Even if we are uncertain about the magnitude and even the sign of the TOA aerosol forcing, we can still make some justified assumptions about the change regional distribution of the aerosol.

We regard this time dependent aerosol climatology as a first step towards a climatology that is useful for climate change studies. We expect that it will be improved by constraints from future observations and it will be updated by inputs from the scientific community. E.g., a comparison with long-term surface radiation observations may lead to further constraints for the aerosol composition and change in areas with high contribution of industrial aerosols. A comparison of model results that this trend in aerosol forcing together with the trend in greenhouse gas forcing and other forcing changes (volcanic aerosol, solar irradiance) as input parameters with the observed temperature record may lead to further constraints for this climatology.

References

Benkovitz, C. M., T. Scholtz, J. Pacyna, L. Tarrason, J. Dignon, E. C. Voldner, P. A. Spiro, J. A. Logan, and T. E. Graedel, Global gridded inventories of anthropogenic emissions of sulfur and nitrogen, *J. Geophys. Res.*, *101*, 29,239–29,253, 1996.

Boden, T. A., G. Marland, and R. J. Andres, Estimates of global, regional, and national annual CO_2 emissions from fossil-fuel burning, hydraulic cement production, and gas flaring: 1950-1992, Technical Report Rep. ORNL/CDIAC-90, NDP-030/R6, Oak Ridge Nat. Lab., Oak Ridge, TN, 600pp., 1996.

Bond, T. C., R. Charlson, and J. Heintzenberg, Quantifying the emission of light-absorbing particles: Measurements tailored to climate studies, *Geophys. Res. Lett.*, *25*, 337–340, 1998.

Charlson, R. J., D. S. Covert, and T. V. Larson, Observation of the effect of humidity on light scattering by aerosols, in *Hygroscopic Aerosols*, edited by L. R. and A. Deepak, pp. 35–44, A. Deepak, Hampton, Va., 1984.

Charlson, R. J., J. Langner, H. Rodhe, C. B. Leovy, and S. G. Warren, Perturbation of the northern hemisphere radiative balance by backscattering from anthropogenic sulfate aerosols, *Tellus*, *43*AB, 152–163, 1991.

Cooke, W. F., C. Liousse, H. Cachier, and H. Feichter, Construction of a 1° × 1° fossil fuel emission data set for carbonaceous aerosol and implementation and radiative impact in the echam4 model, *J. Geophys. Res.*, 1999, in press.

Cooke, W. F., and J. N. Wilson, A global black carbon aerosol model, *J. Geophys. Res.*, *101*, 19,395–19,409, 1996.

Dignon, J., and S. Hameed, Global emissions of nitrogen and sulfur oxides from 1860 to 1980, *J. Air Poll. Con. Assoc.*, *39*, 180–186, 1989.

Hansen, J., M. Sato, and R. Ruedy, Radiative forcing and climate response, *J. Geophys. Res.*, *102*, 6831–6864, 1997.

Hansen, J. E., G. L. Russell, D. Rind, P. Stone, A. Lacis, S. Lebedeff, R. Ruedy, and L. Travis, Efficient three–dimensional global models for climate studies: Models I and II, *Mon. Weather Rev.*, *111*, 609–662, 1983.

Hansen, J. E., M. Sato, A. Lacis, R. Ruedy, I. Tegen, and E. Matthews, Climate forcings in the industrial era, *Proc. Natl. Acad. Sci.*, *22*, 12,753–12,758, 1998.

Hansen, J. E., and L. D. Travis, Light scattering in planetary atmospheres, *Space Sci. Rev.*, *16*, 527–610, 1974.

Haywood, J. M., D. L. Roberts, A. Slingo, J. M. Edwards, and K. P. Shine, General circulation model calculations of the direct radiative forcing by anthropogenic sulfate and fossil fuel soot aerosols, *J. Clim.*, *10*, 1562–1577, 1997.

Haywood, J. M., V. Ramaswamy, and B. J. Soden, Tropospheric aerosol forcing in clear-sky satellite observations over the oceans, *Science*, *283*, 1299–1303, 1999.

Haywood, J. M., and V. Ramaswamy, Global sensitivity studies of the direct radiative forcing due to anthropogenic sulfate and black carbon aerosols, *J. Geophys. Res.*, *103*, 6043–6058, 1998.

Haywood, J. M., and K. P. Shine, The effect of anthropogenic sulfate and soot aerosol on the clear sky planetary radiation budget, *Geophys. Res. Lett.*, *22*, 603–606, 1995.

Hegg, D. A., J. Livingston, P. V. Hobbs, T. Novakov, and P. Russel, Chemical apportionment of aerosol column optical depth off the mid-Atlantic coast of the United States, *J. Geophys. Res.*, *102*, 25,293–25,303, 1997.

Heintzenberg, J., R. J. Charlson, A. D. Clarke, C. Liousse, V. Ramaswamy, K. P. Shine, M. Wendisch, and G. Helas, Measurements and modelling of aerosol single scattering albedo: Progress, problems and prospects, *Beitr. Phys. Atmosph.*, *70*, 249–263, 1997.

Hobbs, P. V., J. S. Reid, R. A. Kotchenruther, R. J. Ferek, and R. Weiss, Direct radiative forcing by smoke from biomass burning, *Science*, *275*, 1776–1778, 1997.

Hollrigl, P., Modelling the distribution of aerosols and their effect on the atmospheric radiation, Ph.D. thesis, ETH Zurich, Switzerland, 1997.

Karl, T. R., R. W. Knight, G. Kukla, and J. Gavin, Evidence for radiative effects of anthropogenic aerosols in the observed climate record, in *Aerosol Forcing of Climate*, edited by R. Charlson, and J. Heintzenberg, 363–382, John Wiley & Sons, New York, 1995.

Kiehl, J. T., and B. P. Briegleb, The relative importance of sulfate aerosols and greenhouse gases in climate forcing, *Science*, *260*, 311–314, 1993.

Kiehl, J. T., and H. Rodhe, Modeling geographical and seasonal forcing due to aerosols, in *Aerosol Forcing of Climate*, edited by R. Charlson, and J. Heintzenberg, pp. 281–296, John Wiley, New York, 1995.

Koch, D., D. Jacob, I. Tegen, D. Rind, and M. Chin, Tropospheric sulfur simulation and sulfate direct radiative forcing in the GISS GCM, *J. Geophys. Res.*, 1999, in press.

Lacis, A. A., and M. I. Mishchenko, Climate forcing, climate sensitivity, and climate response: A radiative modeling perspective on atmospheric aerosols, in *Aerosol Forcing of Climate*, edited by R. Charlson, and J. Heintzenberg, pp. 11–42, John Wiley, New York, 1995.

Lefohn, A. S., J. D. Husar, and R. B. Husar, Estimating historical anthropogenic global sulfur emission patterns for the period 1850-1990, *Atmos. Environ.*, *33*, 3435–3444, 1999.

Liousse, C., J. E. Penner, C. Chuang, J. J. Walton, H. Eddleman, and H. Cachier, A global three-dimensional model study of carbonaceous aerosols, *J. Geophys. Res.*, *101*, 1996, 19,411–19,432.

Malm, W. C., J. F. Sisler, D. Huffman, R. A. Eldred, and T. A. Cahill, Spatial and temporal trends in particle concentration and optical extinction in the United States, *J. Geophys. Res.*, *99*, 1347–1370, 1994.

Mayewski, P. A., W. B. Lyons, M. J. Spencer, M. S. Twickler, C. F. Buck, and S. Whitlow, An ice core record of atmospheric response to anthropogenic sulphate and nitrate, *Nature*, *346*, 554–556, 1990.

Mhyre, G., F. Stordal, K. Restad, and I. S. A. Isaaksen, Estimates of the direct radiative forcing due to sulfate and soot aerosols, *Tellus*, *50B*, 463–477, 1999.

Mosher, B. W., P. Winkler, and J. L. Jaffrezo, Seasonal aerosol chemistry at Dye 3, Greenland, *Atmos. Environ.*, *27A*, 2761–2772, 1993.

Moulin, C., C. E. Lambert, F. Dulac, and U. Dayan, Control of atmospheric export of dust from North Africa by the North Atlantic Oscillation, *Nature*, *387*, 691–694, 1997.

NADP, National acid deposition program, national trends network (nrsp-3), Technical report, NADP Program Office, Illinois State Water Survey, Champaign, Illinois, 1999.

Nilsson, B., Meteorological influence on aerosol extinction in the 0.2–40 mum wavelength range, *Appl. Opt.*, *18*, 3457–3473, 1979.

Patterson, E. M., D. A. Gillette, and B. H. Stockton, Complex index of refraction between 300 and 700 nm for Saharan aerosols, *J. Geophys. Res.*, *82*, 3153–3160, 1977.

Penner, J. E., C. C. Chuang, and K. Grant, Climate forcing by carbonaceous and sulfate aerosols, *Clim. Dyn.*, *14*, 839–851, 1998.

Prospero, J. M., and R. T. Nees, Impact of the North African drought and El Niño on mineral dust in the Barbados trade winds, *Nature*, *320*, 735–738, 1986.

Quinn, P. K., and D. J. Coffman, Comment on "Contribution of different aerosol species to the global aerosol extinction optical thickness: Estimates from model results" by Tegen et al., *J. Geophys. Res.*, 1999.

Roeckner, E., T. Siebert, and J. Feichter, Climatic response to anthropogenic sulfate forcing simulated with a general circulation model, in *Aerosol Forcing of Climate*, edited by R. Charlson, and J. Heintzenberg, 349–362, John Wiley & Sons, New York, 1995.

Sato, M., J. Hansen, M. P. McCormick, and J. B. Pollack, Stratospheric aerosol optical depths, 1850-1990, *J. Geophys. Res.*, *98*, 22,987–22,994, 1993.

Schaug, J., J. E. Hansen, K. Nodop, B. Ottar, and J. M. Pacyna, Summary report from the chemical co-ordinating center for the third phase of emep, Technical Report EMEP/CC Rep. 3/87, Norw. Inst. for Air Res., Lillestrom, 160 pp., 1987.

Schult, I., J. Feichter, and W. F. Cooke, Effect of black carbon and sulfate aerosols on the global radiation budget, *J. Geophys. Res.*, *102*, 30,107–30,117, 1997.

Schulz, M., Y. Balkanski, W. Guelle, and F. Dulac, Role of aerosol size distribution and source location in a three-dimensional simulation of a Saharan dust episode tested against satellite derived optical thickness, *J. Geophys. Res.*, *103*, 10,579–10,592, 1998.

Tegen, I., A. Lacis, and I. Fung, The influence of mineral aerosol from disturbed soils on the global radiation budget, *Nature*, *380*, 419–422, 1996.

Tegen, I., P. Hollrigl, M. Chin, I. Fung, D. Jacob, and J. Penner, Contribution of different aerosol species to the global aerosol extinction optical thickness: Estimates from model results, *J. Geophys. Res.*, *102*, 23,895–23,915, 1997.

Tegen, I., and I. Fung, Modeling of mineral dust in the atmosphere: Sources, transport, and optical thickness, *J. Geophys. Res.*, *99*, 22,897–22,914, 1994.

Tegen, I., and I. Fung, Contribution to the mineral aerosol load from land surface modification, *J. Geophys. Res.*, *100*, 18,707–18,726, 1995.

Tegen, I., and A. A. Lacis, Modeling of particle size distribution and its influence on the radiative properties of mineral dust aerosol, *J. Geophys. Res.*, *101*, 19,237–19,244, 1996.

Toon, J. B., O. B. abd Pollack, and B. N. Khare, The optical constants of several atmospheric aerosol species: Ammonium sulfate, aluminum oxide, and sodium cloride, *J. Geophys. Res.*, *81*, 5733–5748, 1976.

United Nations, The united nations energy statistica database (1994), Technical report, United Nations Statistics Division, 1996.

Volz, F. E., Infrared optical constants of ammonium sulfate, Sahara dust, volcanic pumice, and flyash, *Appl. Optics*, *12*, 564–568, 1973.

This manuscript was prepared with the AGU LaTeX macros v3.0.

Table 1. Global Average Optical Thickness, Single Scattering Albedos at the Reference Wavelength $\lambda = 0.55\mu$m, and Nominal Particle Radius for the Individual Tropospheric Aerosol Types

Aerosol Type	Optical Thickness	ω_0	r_{eff}
Sulfate (Fossil Fuel) 1990	0.0044-0.0222 (0.0111)	1.00	1.0
Sulfate (Fossil Fuel) 1950	0.0018-0.0090 (0.0045)	1.00	1.0
BC (Fossil Fuel) 1990	0.0013-0.0067 (0.0034)	0.31	0.1
BC (Fossil Fuel) 1950	0.0004-0.0021 (0.0011)	0.31	0.1
OC (Fossil Fuel) 1990	0-0.0267 (0.0134)	0.96	0.5
OC (Fossil Fuel) 1950	0-0.0086 (0.0043)	0.96	0.5
Sulfate (Natural)	0.0067	1.00	0.3
Biomass Burning BC	0.0014	0.48	0.5
Biomass Burning OC	0.0124	0.93	1.0
Natural Organics	0.0032	0.98	0.3
Soil Dust	0.0324	0.89	*)
Sea Salt	0.0267	1.00	2.0

*) 8 individual size ranges (see *Tegen and Lacis* [1996])

Table 2. Radiative Forcing for Different Scenarios

Scenario	Year	AOT (Fossil Fuel)	ω_0 (All Aerosol)	TOA Forcing (W m^{-2})	Atmos. Heating (W m^{-2})
FF 90	1990	0.039	0.945	-0.27	1.37
FF 80	1980	0.029	0.948	-0.24	0.91
FF 70	1970	0.024	0.949	-0.19	0.67
FF 50	1950	0.014	0.949	-0.10	0.38
Max C	1990	0.056	0.934	0.12	2.31
Min C	1990	0.029	0.954	-0.51	0.80
Max τ	1990	0.064	0.945	-0.38	1.77
Min τ	1990	0.024	0.945	-0.15	0.77
All A	1990	0.069	0.945	0.05	2.48
All T	1990	0.122	0.945	-0.85	2.70

Figure captions:

Figure 1: Emissions of SO_2 (in Mt S/yr) (a) and BC aerosols (b,c) (in Mt C/yr) from 1950 to 1990. Shown are global averages, uncertainty ranges and emissions for the U.S. and China.

Figure 2: Ratio of annual S and BC emissions for 1950 to 1990 for the global average, for the examples of the U.S and China, and the global average for the case that the shift between domestic and industrial fuel burning was not taken into consideration.

Figure 3: Comparison of modeled sulfur deposition with measurements at NADP in the U.S. sites from 1979 to 1990, deposition fluxes are in (mg S m^{-2} yr^{-1})

Figure 4: Comparison of sulfate concentration trends in the model with measurements at EMEP sites in Europe, compared are the trends for all stations (3a) and central and northern European sites separately (3b).

Figure 5: Comparison of modeled BC concentrations with measurements summarized by *Liousse et al.* [1996] (5a) and modeled BC and OC concentrations measurements from the IMPROVE network sites [*Malm et al.*, 1994] (5b) for the case of "moderate" carbonaceous aerosol.

Figure 6: Modeled tropospheric aerosol optical thickness for the years 1950, 1970, and 1990.

Figure 7: Trend in aerosol optical thickness for fossil fuel sulfate, BC and OC for the global average and the examples of U.S. and China.

Figure 8: Comparison of modeled tropospheric aerosol single scattering albedo with northern hemisphere measurements summarized by *Heintzenberg et al.* [1997] (asterisks), from TARFOX [*Hegg et al.*, 1997] (open circle), and from SCAR-B [*Hobbs et al.*, 1997] (plus signs). The error bars indicate the range obtained for the "maximum" and "low" fossil fuel carbonaceous aerosol cases.

Figure 9: Global distributions of annual averaged single scattering albedos for the cases

of "maximum", "moderate", and "low" contribution of fossil fuel carbonaceous aerosols.

Figure 10: Change in and annually averaged tropospheric aerosol single scattering albedos for the global mean and the examples of U.S. and China.

Plate 1 : Annually averaged optical thickness ($\times$ 100) distributions for the various tropospheric aerosol types for the year 1990.

Plate 2 : Seasonal variation of modeled aerosol optical thickness between 1950 and 1990.

Plate 3 : Net TOA radiative forcing for 1980 for "moderate" fossil fuel carbonaceous aerosol contribution (a); and the change between 1970 and 1990 occurring for the cases of "maximum" and "low" fossil fuel carbonaceous aerosol.

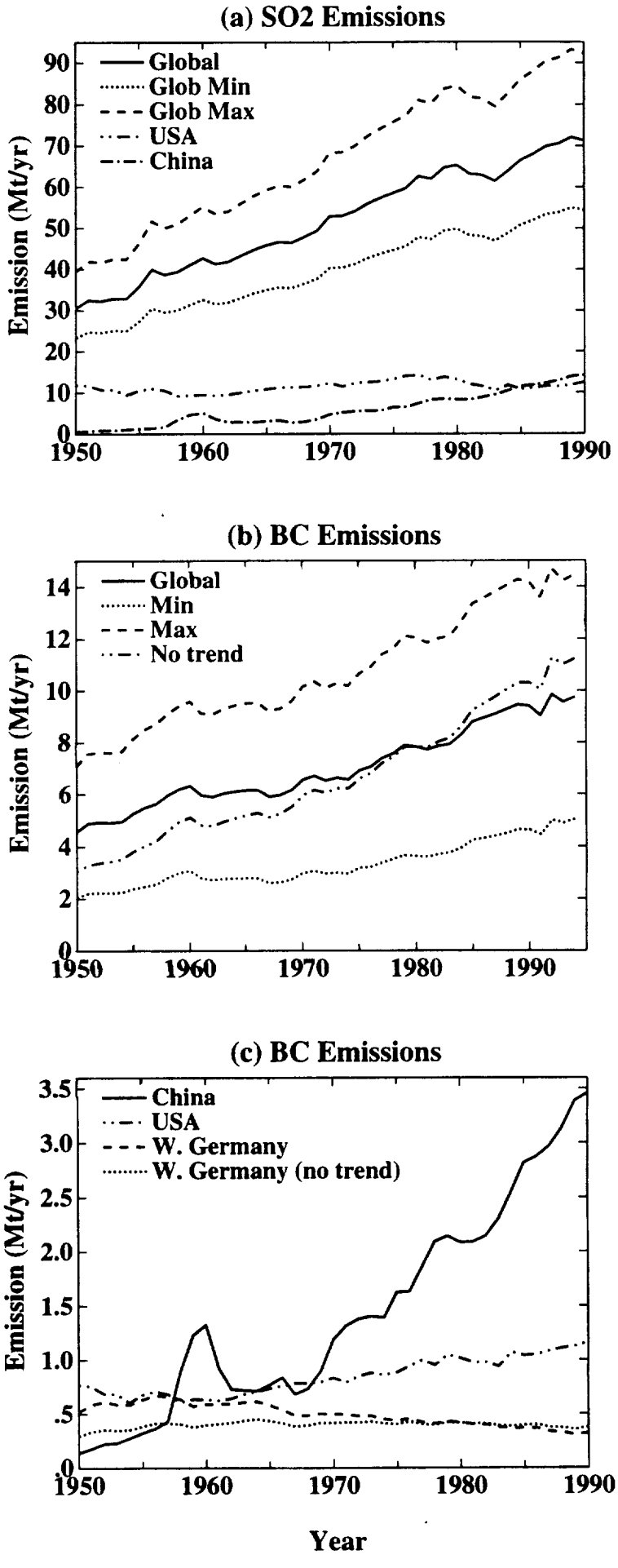
(a) SO2 Emissions
Global
Glob Min
Glob Max
USA
China
Emission (Mt/yr)
0
10
20
30
40
50
60
70
80
90
1950
1960
1970
1980
1990
(b) BC Emissions
Global
Min
Max
No trend
Emission (Mt/yr)
0
2
4
6
8
10
12
14
1950
1960
1970
1980
1990
(c) BC Emissions
China
USA
W. Germany
W. Germany (no trend)
Emission (Mt/yr)
0
.5
1.0
1.5
2.0
2.5
3.0
3.5
1950
1960
1970
1980
1990
Year

Fig. 1

Fig. 2

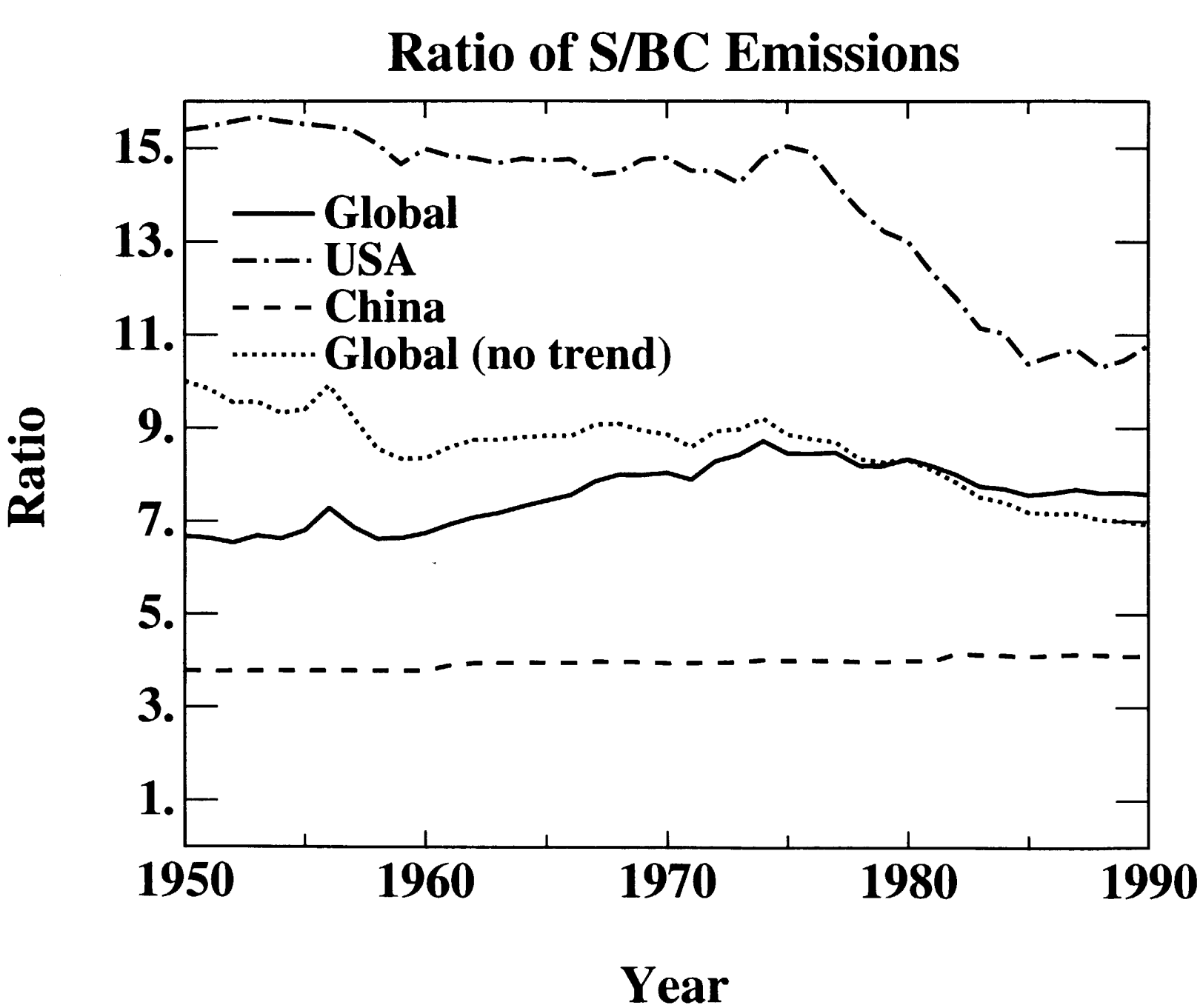
Ratio of S/BC Emissions
Global
USA
China
Global (no trend)
Ratio
15.
13.
11.
9.
7.
5.
3.
1.
1950
1960
1970
1980
1990
Year

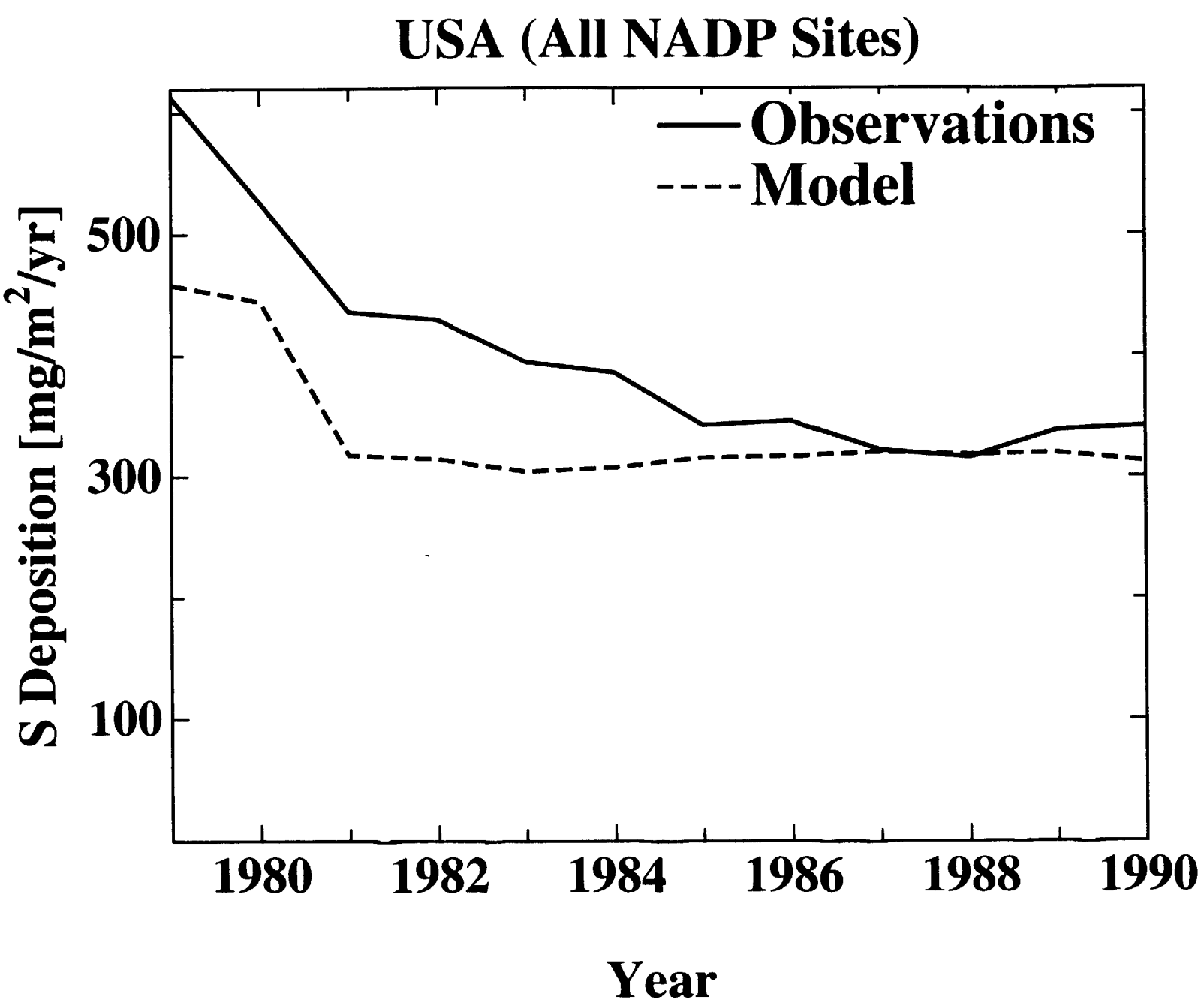
USA (All NADP Sites)
Observations
Model
S Deposition [mg/m^2/yr]
500
300
100
1980
1982
1984
1986
1988
1990
Year

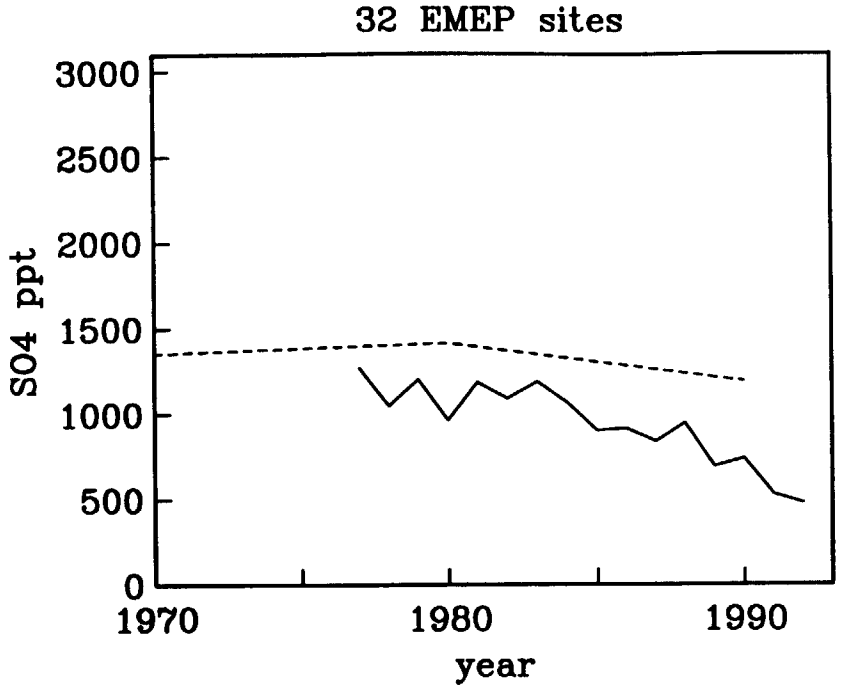
32 EMEP sites
3000
2500
2000
1500
1000
500
0
SO4 ppt
1970
1980
1990
year

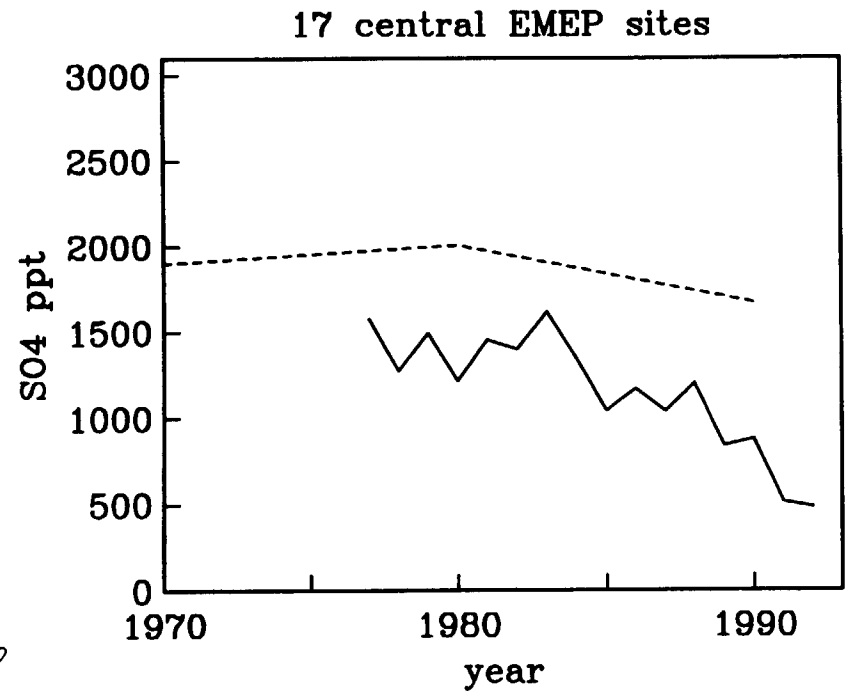
17 central EMEP sites
3000
2500
2000
1500
1000
500
0
SO4 ppt
1970
1980
1990
year

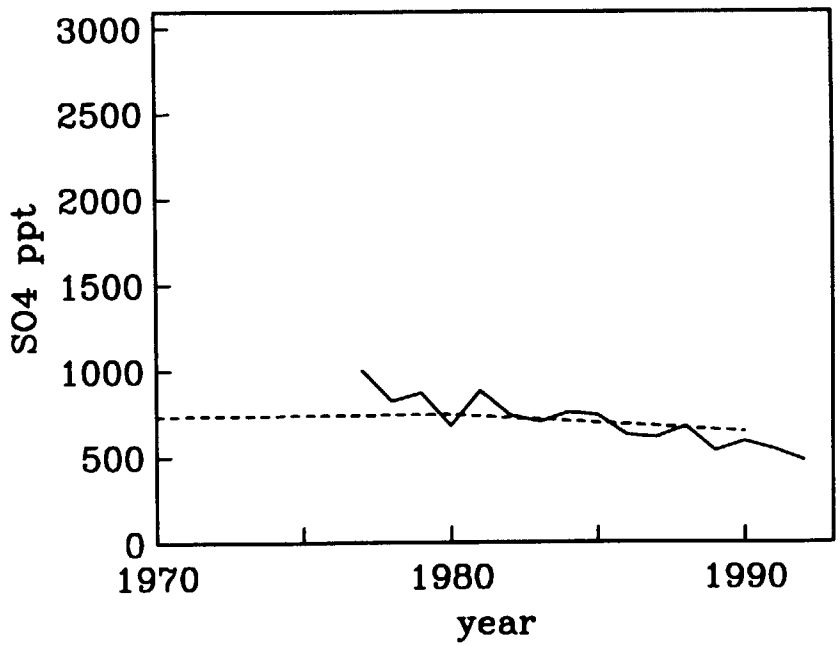
15 northern EMEP sites
3000
2500
2000
1500
1000
500
0
SO4 ppt
1970
1980
1990
year

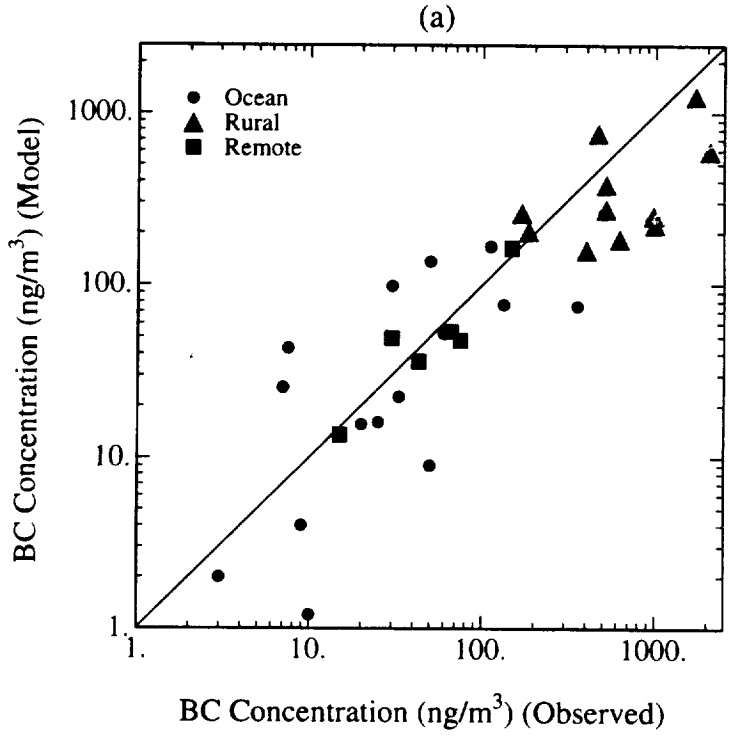
(a)
Ocean
Rural
Remote
1000.
100.
10.
1.
1.
10.
100.
1000.
BC Concentration (ng/m3) (Model)
BC Concentration (ng/m3) (Observed)

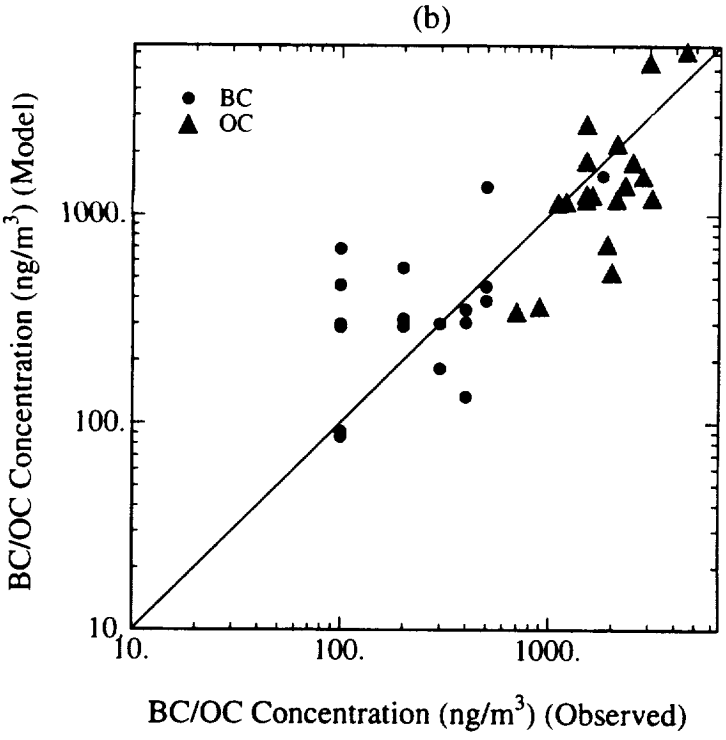
(b)
BC
OC
1000.
100.
10
10.
100.
1000.
BC/OC Concentration (ng/m3) (Model)
BC/OC Concentration (ng/m3) (Observed)

Fig. 5

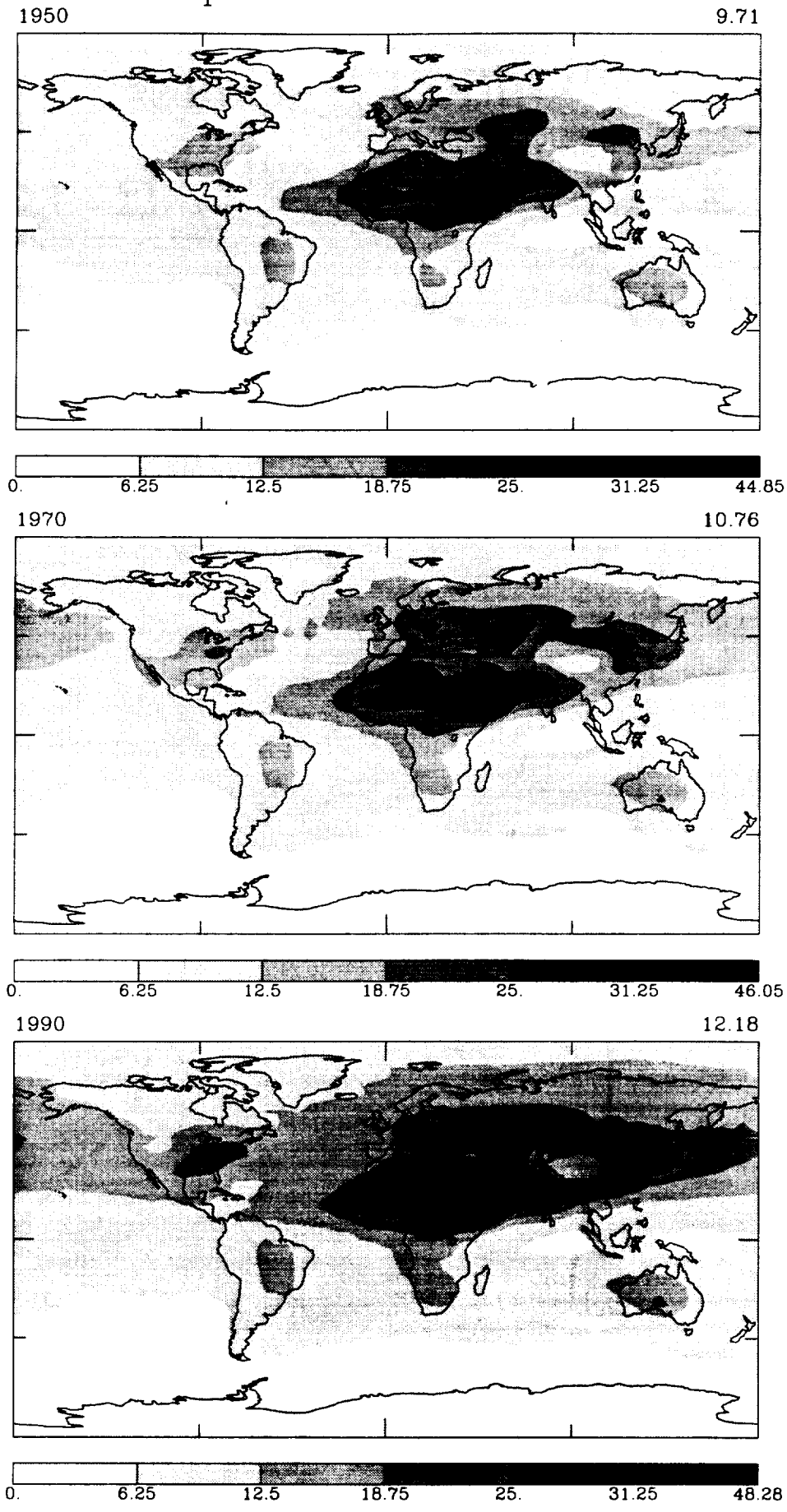
Optical Thickness x 100
1950
9.71
0.
6.25
12.5
18.75
25.
31.25
44.85
1970
10.76
0.
6.25
12.5
18.75
25.
31.25
46.05
1990
12.18
0.
6.25
12.5
18.75
25.
31.25
48.28

Fig. 6

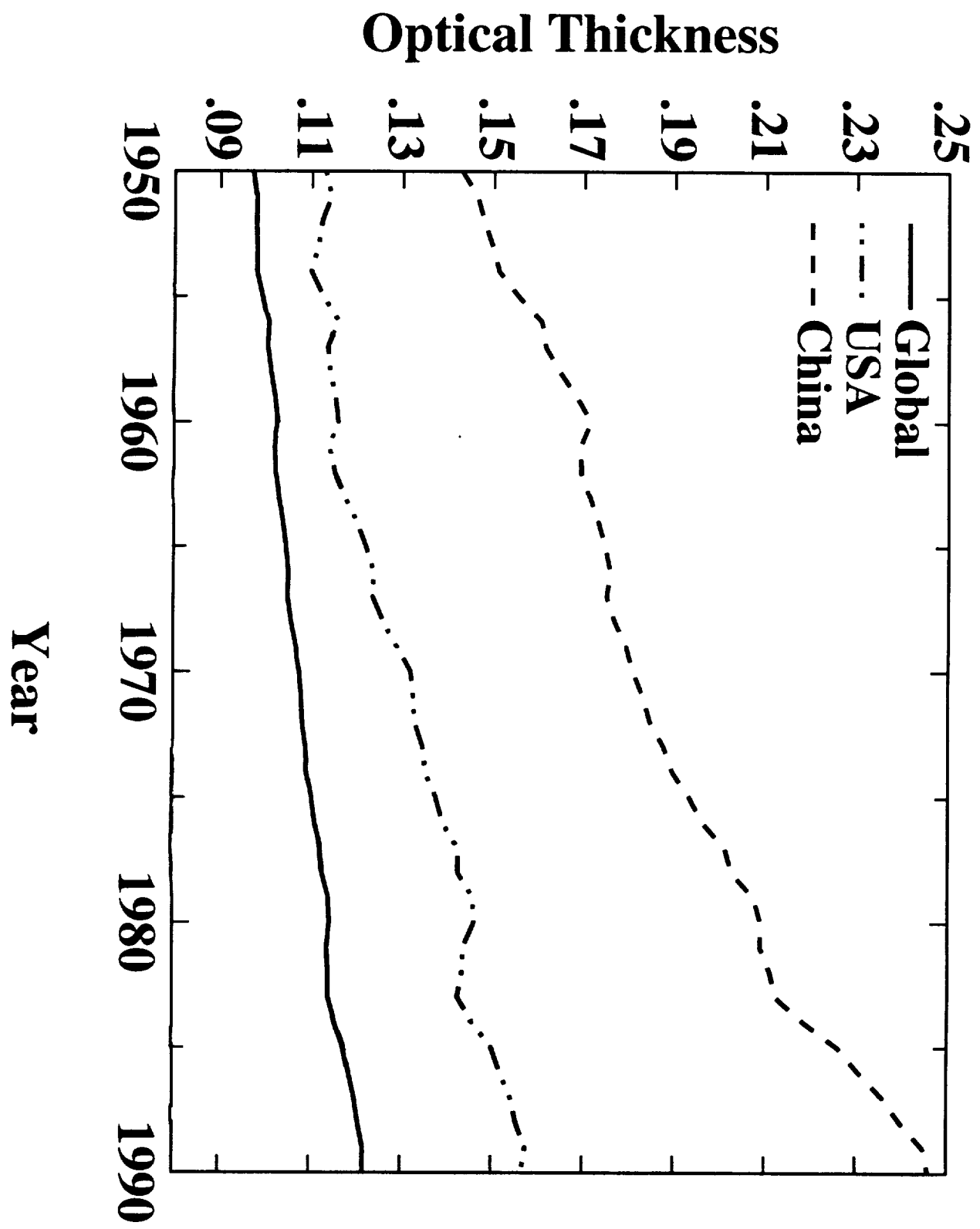
Optical Thickness
.09
.11
.13
.15
.17
.19
.21
.23
.25
1950
1960
1970
1980
1990
Year
Global
USA
China

Fig. 7

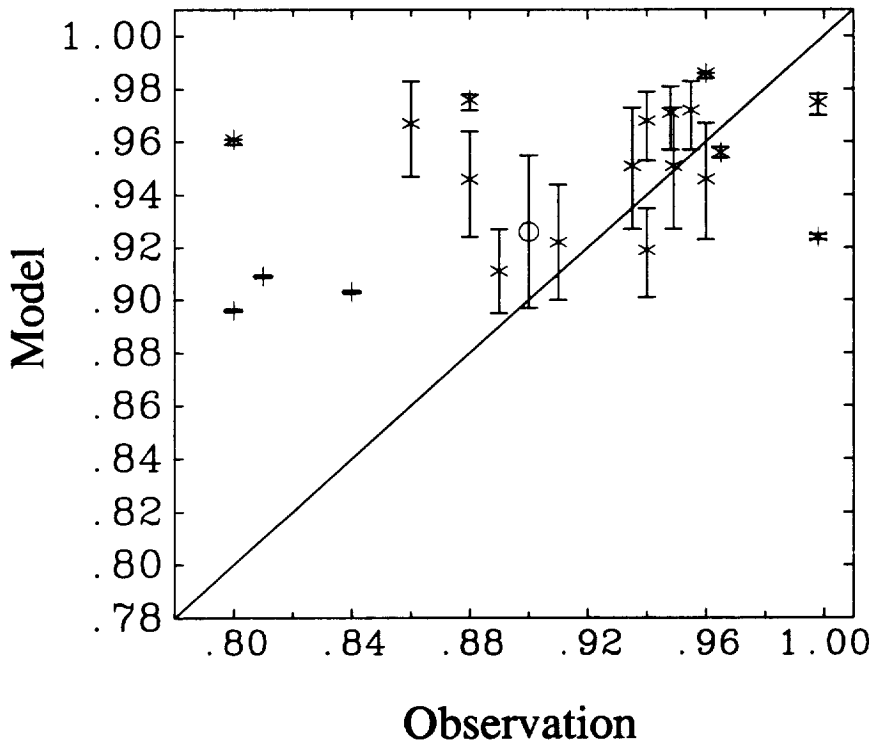
1.00
.98
.96
.94
.92
.90
.88
.86
.84
.82
.80
.78
Model
.80
.84
.88
.92
.96
1.00
Observation

Fig 8

Single Scattering Albedo

Max. BC 0.93

0.88 0.9 0.92 0.94 0.96 0.98 1.

BC x 0.5 0.94

0.88 0.9 0.92 0.94 0.96 0.98 1.

BC x 0.2 0.95

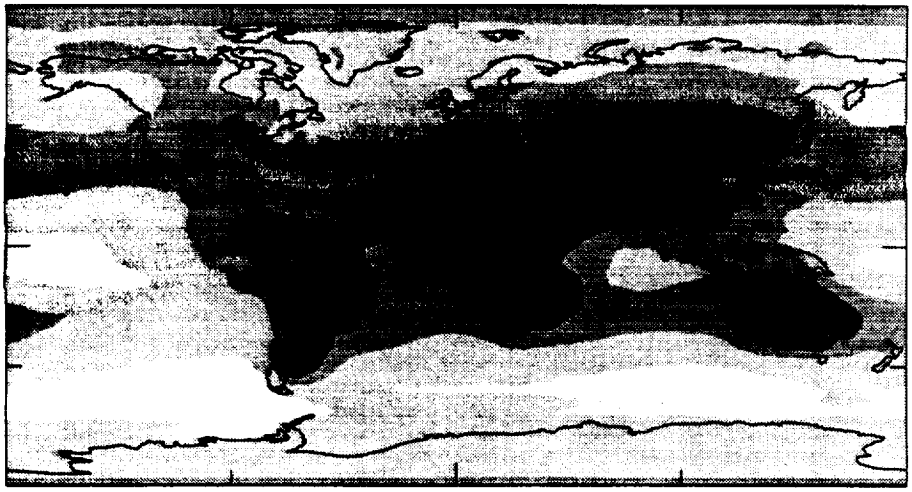

0.88 0.9 0.92 0.94 0.96 0.98 1.

Fig. 7

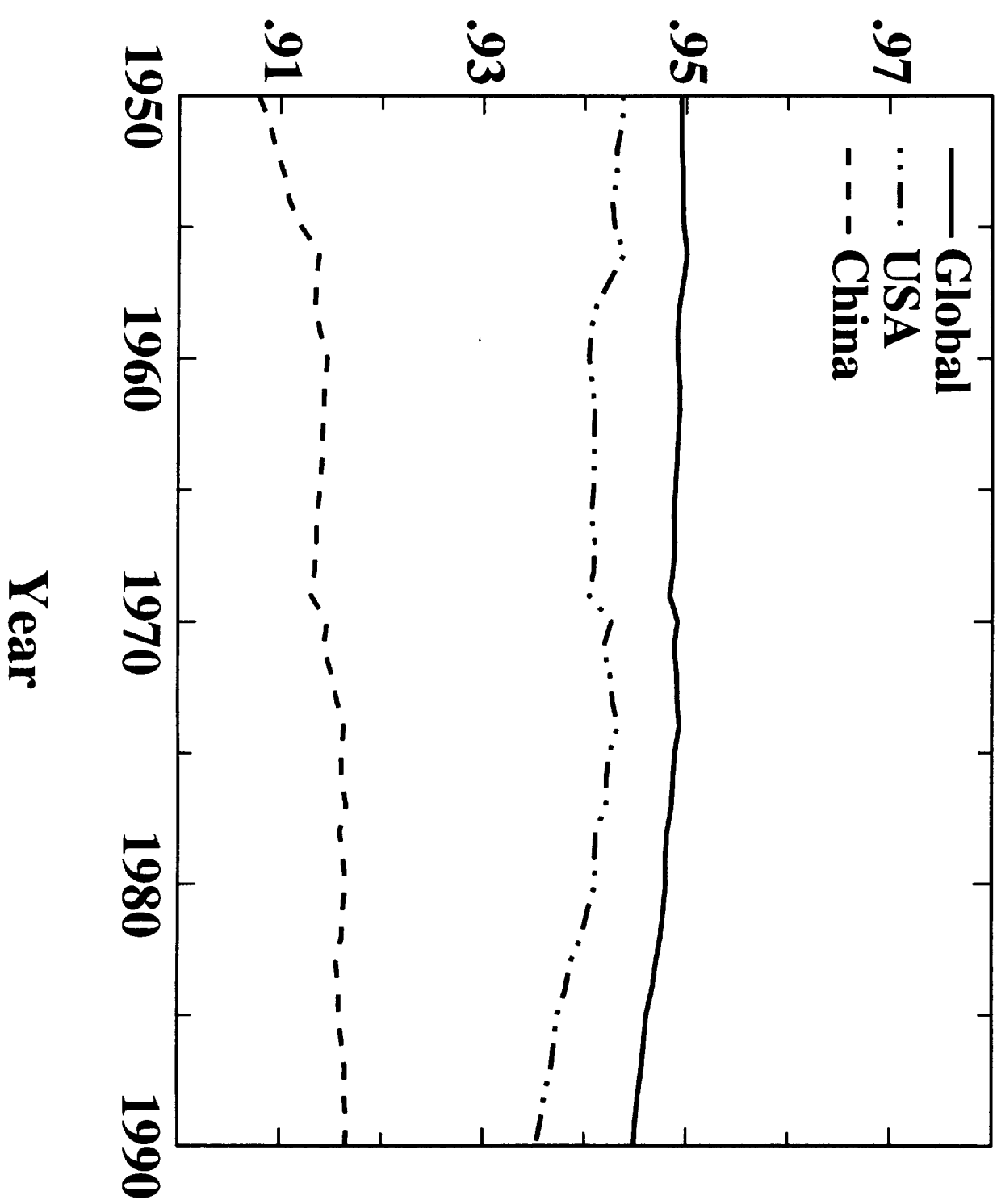
Single Scattering Albedo
.91
.93
.95
.97
1950
1960
1970
1980
1990
Year
Global
USA
China

Fig. 10

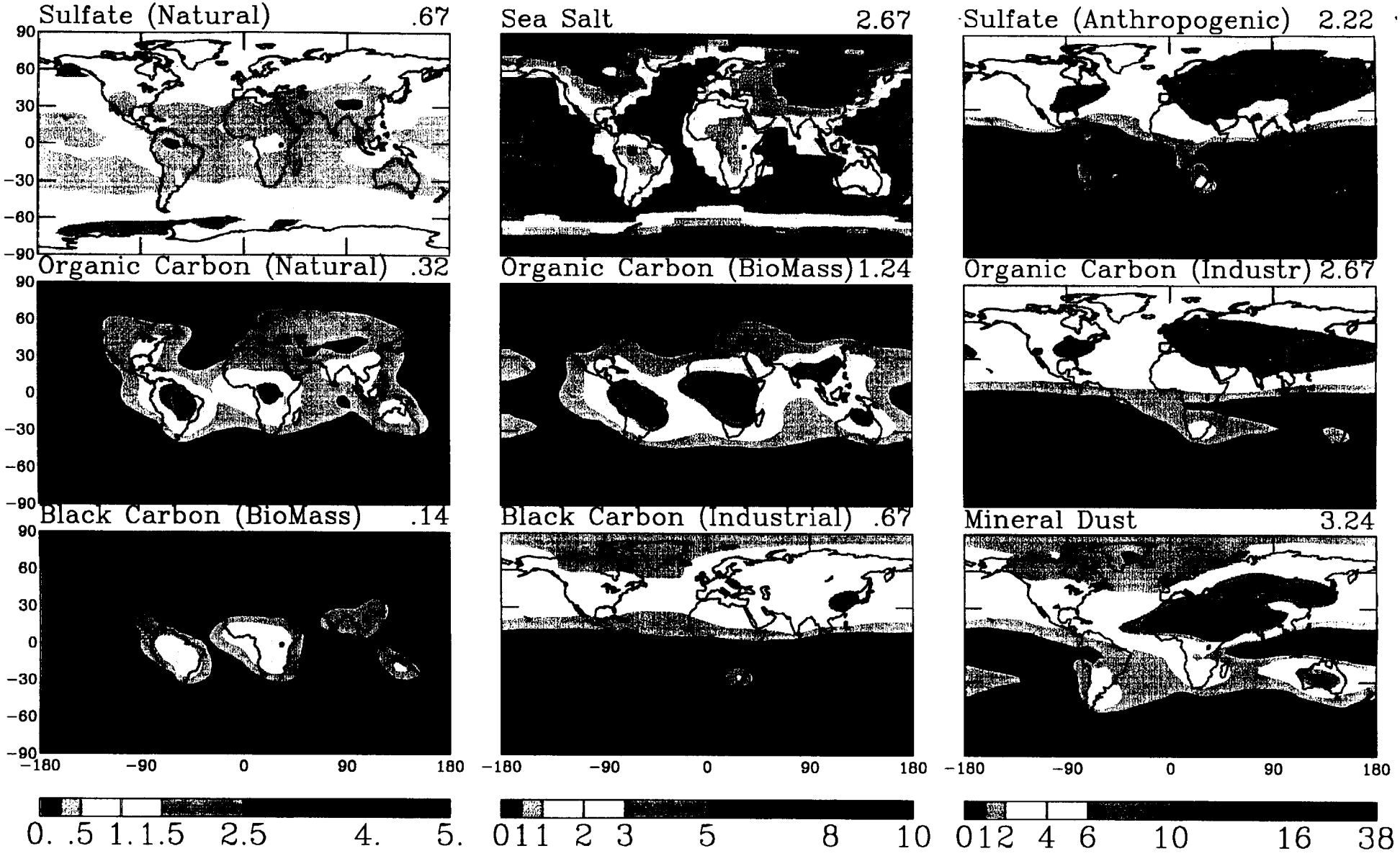
Sulfate (Natural) .67
Sea Salt 2.67
Sulfate (Anthropogenic) 2.22
Organic Carbon (Natural) .32
Organic Carbon (BioMass) 1.24
Organic Carbon (Industr) 2.67
Black Carbon (BioMass) .14
Black Carbon (Industrial) .67
Mineral Dust 3.24
90
60
30
0
-30
-60
-90
-180
-90
0
90
180
0. .5 1. 1.5 2.5 4. 5.
0 1 1 2 3 5 8 10
0 1 2 4 6 10 16 38

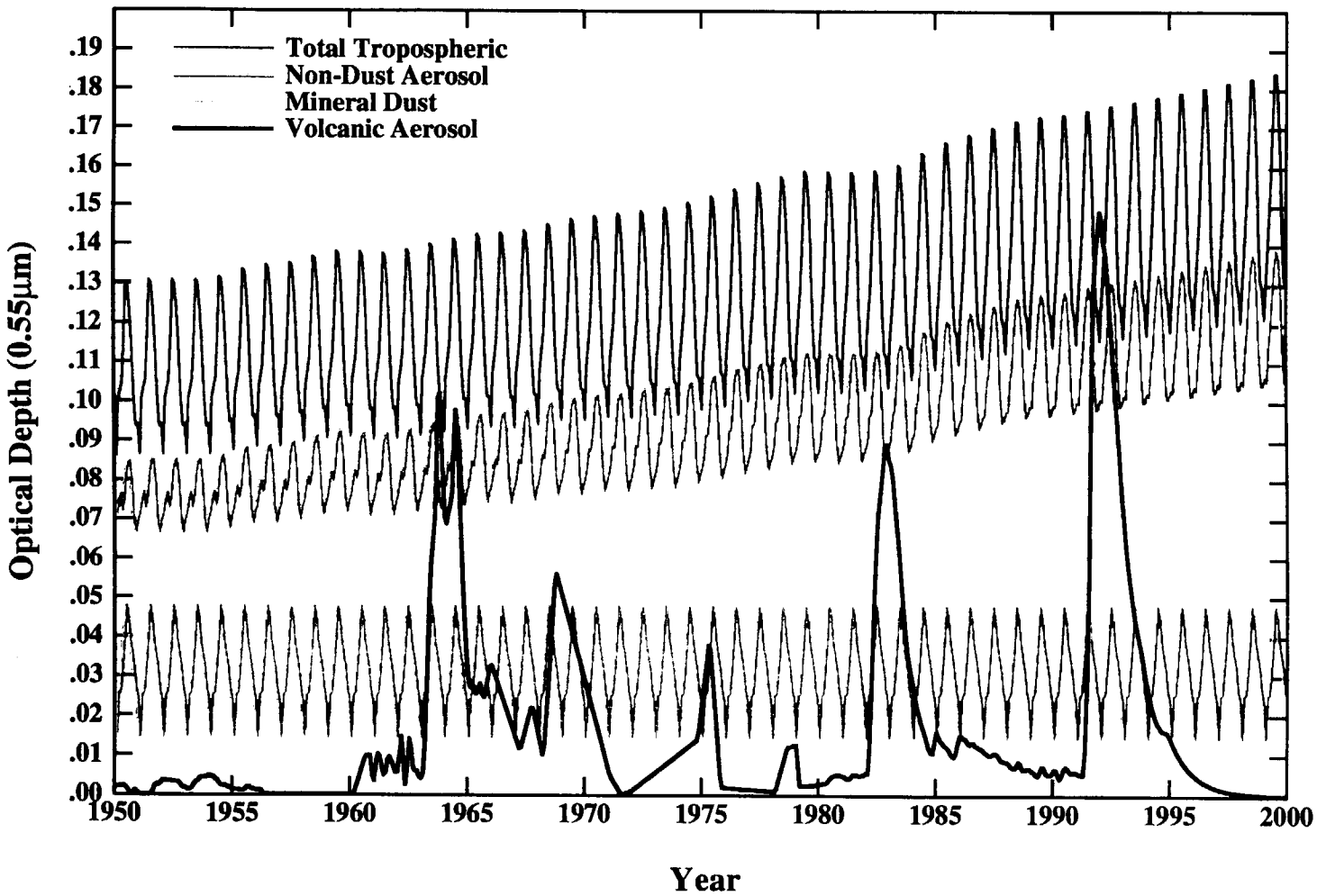
Total Tropospheric
Non-Dust Aerosol
Mineral Dust
Volcanic Aerosol
Optical Depth (0.55μm)
.19
.18
.17
.16
.15
.14
.13
.12
.11
.10
.09
.08
.07
.06
.05
.04
.03
.02
.01
.00
1950
1955
1960
1965
1970
1975
1980
1985
1990
1995
2000
Year

TOA Net Radiative Forcing (W m^{-2})

1980 (BC x 0.5) −0.24 W m^{-2}

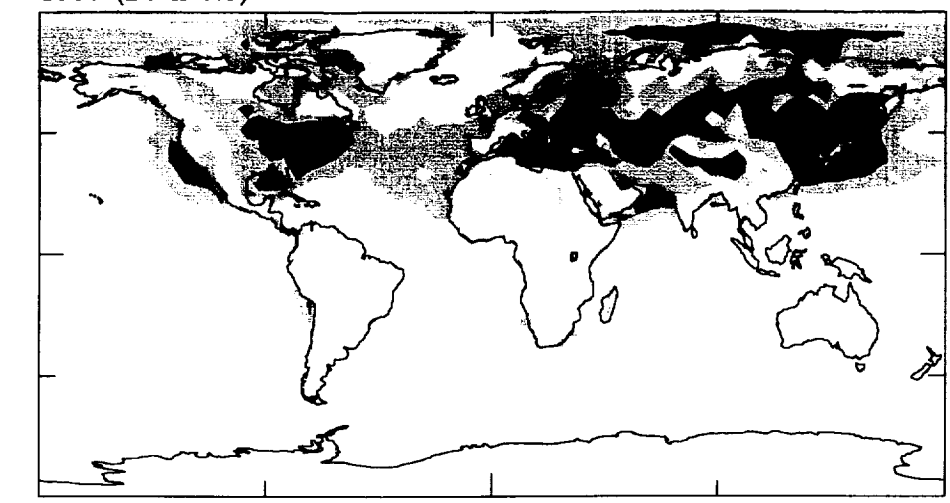

−3.1 −1.8 −1.4 −1 −0.6 −0.2 0.2 0.6 1.0 1.4 1.8 3.0

1990 minus 1970, BC max 0.11 W m^{-2}

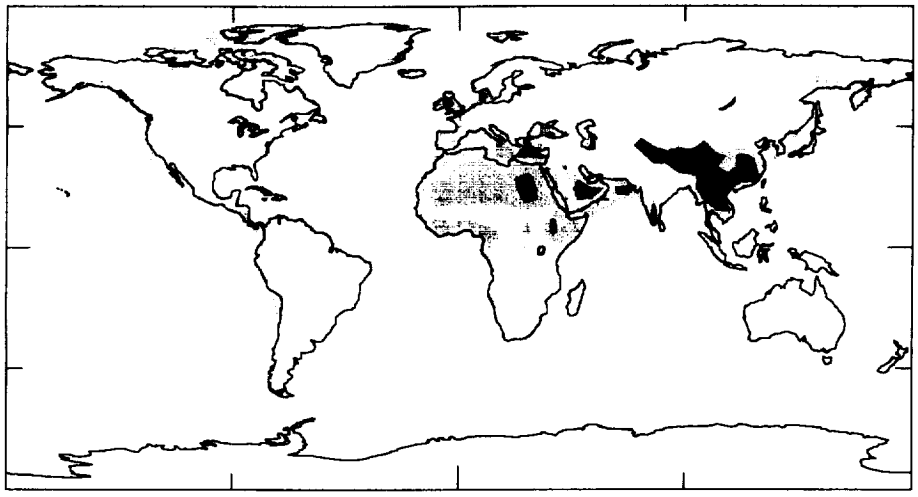

−2.2 −1.8 −1.4 −1 −0.6 −0.2 0.2 0.6 1.0 1.4 1.8 4.2

1990 minus 1970, BC x 0.2 −0.19 W m^{-2}

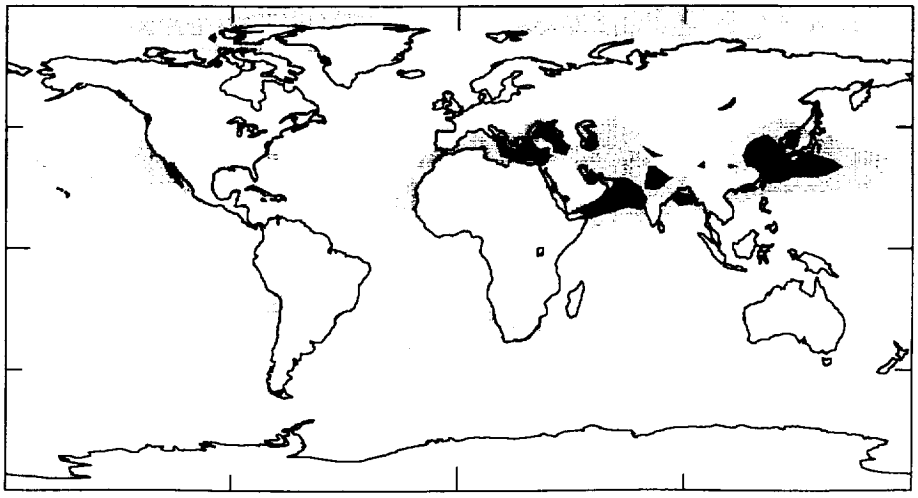

−2.2 −1.8 −1.4 −1 −0.6 −0.2 0.2 0.6 1.0 1.4 1.8 2.2

Fig 3